A PROPOSED CONTROLLER-BASED FREE-SPACE OPTICAL NETWORK ARCHITECTURE WITH LAGRANGE POINT RELAYS FOR EARTH-MARS COMMUNICATION

by
Nicholas D. Zayfman

A thesis submitted to The Johns Hopkins University in conformity with the requirements for the degree of Master of Science in Engineering in Computer Science

Baltimore, Maryland
October 2025

Abstract

Current interplanetary communications face severe limitations including bandwidth constraints, solar conjunction blackouts lasting up to two weeks, and infrastructure unable to support exponential growth in mission data requirements. This thesis presents a simulation-based feasibility study of a hierarchical controller-based free-space optical (FSO) communication architecture leveraging strategic Lagrange point positioning to address these challenges. The proposed system integrates three architectural innovations: (1) controller satellites at Earth-Moon Lagrange points (L_3, L_4, L_5) providing centralized navigation assistance and traffic coordination, (2) relay satellites at Sun-Earth and Sun-Mars Lagrange points enabling communication paths around solar occlusion, and (3) FSO-equipped access satellites at Earth and Mars for high-bandwidth data transmission.

Through parametric simulation spanning 2.28 years with 8 Earth satellites, 4 Mars satellites, 3 controllers, and 8 relays, the controller-based architecture demonstrates 100% connectivity and 31-37 Gbps aggregate capacity—a 5-16× improvement over current capabilities. Controllers enable 55% higher throughput (31.978 Gbps vs 20.215 Gbps baseline) through coordinated link management affecting 25.4% of connections. Geometric analysis confirms L_4/L_5 relay positioning maintains line-of-sight during conjunction when direct paths are blocked.

Critical assumptions require experimental validation: navigation-assisted pointing improvements (50% acquisition time reduction, 2 dB SNR enhancement), controller

coordination effectiveness across 4-24 minute light-time delays, and FSO parameters (80% optical efficiency, 30 μrad beam divergence) represent engineering targets rather than validated performance. The simulation establishes architectural feasibility while identifying key validation requirements for operational deployment.

Keywords: Lagrange Point Relays, Solar Conjunction Mitigation, FSO Network Simulation, Hierarchical Architecture, Interplanetary Connectivity

Primary reader and thesis advisor

Dr. Krishan Sabnani
Professor
Department of Computer Science
Johns Hopkins University, Baltimore MD

This thesis is dedicated to my beloved wife, Grace, whose unwavering support has been my foundation throughout this journey; to my family, for their constant encouragement; and to my grandfather, Yuri, who handcrafted parts for the Russian space program, taught me the patience that has guided this work, and sadly passed away during its course.

Acknowledgement

I would like to express my sincere gratitude to Dr. Krishan Sabnani for his invaluable guidance throughout this research process. His mentorship, expertise, and unwavering support have been instrumental in the successful completion of this thesis. I am especially inspired by his passion for learning and his deep curiosity, which motivated me to commit wholeheartedly to this research topic and approach each challenge with a sense of purpose and enthusiasm.

I am deeply grateful to Dr. Vint Cerf, whose captivating lecture at the Naval Academy first introduced me to the fascinating field of Interplanetary Internet. His pioneering work and visionary insights sparked my interest in this area of research and inspired me to pursue this thesis topic.

I would also like to thank Dr. Thierry E. Klein, President of Bell Labs Solutions Research at Nokia, for taking the time to engage with my research. The opportunity to present my work to him provided valuable perspectives that enriched this study.

Finally, I extend my appreciation to Johns Hopkins University for providing access to essential research resources and academic papers that formed the foundation of my literature review and theoretical framework.

Scientists discover the world that exists; engineers create the world that never was.

– Theodore von Kármán

Table of Contents

List of Tables

List of Figures

Chapter 1

The Need for a New Space Communications Architecture

1.1 Introduction

NASA projects that in the 2030's the first human expedition will arrive on Mars. [1] The crew will face a sobering reality: their carefully crafted and inspiring message such as "Mission Control, touchdown confirmed. Humanity now walks on two worlds" will take between 4 and 24 minutes to reach Earth, depending on the orbital positions of the planets. Any response, whether a congratulations or an execution of a critical emergency protocol, will take just as long to arrive. This is not due to a limitation of our technology, but to physics itself since all electromagnetic radiation travel at a finite speed across the vacuum of space. This constraint is only the tip of the iceberg that threatens space communication and hinders humanity's expansion beyond Earth.

This thesis explores these challenges through parametric simulation to assess architectural feasibility rather than to validate deployment-ready specifications. The simulation employs engineering estimates for key performance parameters that would require both hardware validation and further in-depth simulation before operational deployment. While the research explores Free Space Optical (FSO) technology as the primary physical layer protocol, the fundamental contribution lies in the network architecture itself—specifically, how strategic positioning of relay and controller satellites at Lagrange points enables continuous connectivity despite changing orbital

geometries while offering autonomous network functionality through controllers.

Humanity is on the threshold of becoming a multiplanetary species. From the first person in space in 1961 to the first moon landing in 1969, our ambitions since then have grown exponentially. This trajectory continues today, with NASA planning 28 missions over the next decade. [2] These modern missions will generate unprecedented amounts of data. Spacecraft now carry high-resolution cameras, spectrometers, and sensors that produce terabytes of information per minute. [3] This challenge extends beyond robotic explorers and includes future Mars colonies that will demand continuous high-bandwidth connectivity for operational telemetry. It is not beyond imagination that the future will hold a coordinated fleet of satellites, rovers, and drones that each will contribute with their own streams of data. However, the limited infrastructure supporting all this communication relies on radio technology that, despite improvements in efficiency and design, still faces the same fundamental limitations of distance and power that constrained the Apollo era.

This chapter analyzes the limitations of current space communication systems and establishes the need for new approaches to meet the demands of future missions. We begin in Section 1.2 by exploring three dimensions of the problem: the exponential growth in data generation from modern space missions, the fundamental limitations of radio-frequency communications, and the challenges posed by deep space exploration and Mars colonization. Section 1.3 defines the research objectives and scope of this thesis that establish boundaries for our investigation. Section 1.4 outlines our research methodology and Section 1.5 provides an outline for the remainder of this thesis. Collectively, these sections explore whether a hierarchical FSO network architecture

that leverages relay satellites at Mars-Sun and Earth-Sun Lagrange points, controller coordination at Earth-Moon Lagrange points, and navigation-assisted pointing could provide continuous high-bandwidth interplanetary communications between Earth and Mars.

The limitations of radio-based space communications are not only technical hurdles, but fundamental constraints on humanity's expansion into the solar system. This thesis focuses on FSO networks as the primary physical network protocol solution. The future of interplanetary communications will involve varying technologies, including proposed hybrid RF / optical systems that take advantage of the strengths of each technology, distributed relay networks that create the backbone of the interplanetary Internet, advanced compression algorithms, AI-driven data prioritization, and quantum key distribution for security.

As governments and private corporations allocate time and resources for space exploration, our communication capabilities will significantly influence the missions we can undertake and their execution. The challenge isn't just technical but conceptual. We must re-imagine how we explore and operate when real-time control is improbable and under the premise that every bit of data is critical. An instrumental part of this re-imagining involves strategic positioning of relay satellites and controllers at Lagrange points which are locations in space where gravitational forces create generally stable positions relative to two celestial bodies. Lagrange points constitute regions of dynamic stability within the complex orbital environment in which planets, satellites, and spacecraft interact gravitationally. These locations can be used for relays in order to communicate around the Sun or intelligent controllers that maintain information of

full network topology.

In addition, FSO communication provides a solution to bandwidth constraints. In contrast to radio waves that disseminate energy over broad beams, FSO systems utilize lasers to generate small, focused beams that measure microradians in width. The concentration of energy, along with the extensive bandwidth at optical frequencies (which includes tens of terahertz compared to hundreds of megahertz for RF), facilitates data speeds that substantially exceed those of RF systems. All while employing smaller and lighter terminals. The Deep-space Optical Terminals (DOT) study showed that a 22-cm diameter optical telescope could achieve 250 Mb/s from Mars distance (0.42 AU). However these narrow optical beams also create new challenges in pointing, acquisition, and tracking that must be solved for a practical deployment. [4]

This thesis addresses one critical component of the re-imagining, which is to provide the design and simulation-based feasibility of an FSO network architecture that leverages Lagrange point relay and controller satellites to create an interplanetary satellite network. This thesis investigates whether combining the bandwidth advantages of optical communications with strategic positioning at Lagrange points and intelligent autonomous coordination could address the fundamental communication bottlenecks limiting deep space exploration. Through simulation-based analysis, we explore the feasibility of maintaining continuous Earth-Mars connectivity using a hierarchical FSO network architecture.

1.2 Research Motivation and Problem Statement

1.2.1 Exponential growth in space mission data requirements

1.2.1.1 The Data Explosion

Modern space missions generate data at extraordinary rates that are driven by technological innovations in sensor miniaturization, increased resolution capabilities, and the adaptation of scientific instruments to space environments. While early Mars rovers like Sojourner (1997) carried just 3 cameras and basic instruments, today's rovers like the Perseverance feature 23 cameras and sophisticated scientific payloads capable of producing gigabytes of high-resolution imagery and sensor data daily. [5] [6] As Dr. Justin Maki, the Perseverance imaging scientist at the Jet Propulsion Laboratory, said, "Cameras are capable of acquiring much more data than can be sent back to Earth," creating a critical bottleneck where rovers must carefully prioritize which data to transmit and discard valuable scientific observations due to bandwidth limitations. [7] Each successive generation of spacecraft has an increase in data generation capabilities, yet the communication infrastructure has not kept pace with this growth.

The Perseverance rover can theoretically generate gigabytes of data daily, however, its transmission capabilities to Earth are severely limited. The rover must store data onboard and carefully prioritize which information to transmit during communication windows. Direct-to-Earth communication is severely constrained by distance and power limitations, while relays through Mars orbiters provide significantly higher data rates of 8-256 kbps (with next-generation systems reaching up to 1 Mbps) for

limited periods during orbital passes. With Earth-Mars distances of up to 400 million kilometers, these transmissions can take over 22 minutes one way to reach Earth. [8] To put this in perspective, the Perseverance generates enough data to fill a smartphone in hours, but takes months to transmit the equivalent amount.

This data bottleneck is not merely a matter of patience. Fundamentally, it limits scientific discovery. For example, Perseverance's SHERLOC instrument can perform a detailed spectroscopic analysis that looks for organic molecules and can generate spatially resolved chemical maps using fluorescence and Raman spectroscopy coupled with microscopic images. [9] Yet the rover faces severe transmission constraints, its primary UHF antenna can send data at a maximum rate of only two megabits per second, and communication windows with orbiters are extremely limited and can transmit data about 10 or 11 hours per day. [10] [11] Scientists often settle for compressed previews and make critical decisions about which samples warrant detailed analysis based on limited information.

This disparity between data generation and transmission capacity creates a fundamental challenge. As researchers note, instruments are capable of collecting much more data than it is practicable to return to Earth, which require systems that assist in image compression and prioritization of data transmission from Mars to Earth. [12] The Mars 2020 Engineering Cameras alone can generate tens of gigabytes of data, yet bandwidth limitations mean potential discoveries in Martian geology, signs of past life, or unexpected phenomena may remain unanalyzed in the rover's memory, never reaching Earth for study. [13]

Future missions promise to exacerbate this data-bandwidth gap. Next-generation Mars missions are planned with hyperspectral imagers that can produce gigabytes per observation, ground-penetrating radar systems that can generate volumetric data sets, and networked surface stations that can create continuous environmental monitoring streams. The Europa Clipper, scheduled to study Jupiter's moon Europa, will carry nine scientific instruments capable of generating multiple gigabytes per flyby, yet must transmit this data across hundreds of millions of kilometers, and face even more severe communication constraints than Mars missions. [14] [15]

This exponential growth in data generation across all mission types, from Mars surface operations producing orders of magnitude more data than can be transmitted, to deep space missions struggling with extreme distances, to even near-Earth telescopes operating at capacity, demonstrates that traditional point-to-point communication architectures are reaching their limits. The disparity between data generation and transmission capabilities threatens to bottleneck scientific discovery, as missions must increasingly make difficult choices about which data to preserve and transmit versus which to discard forever. As missions become more ambitious and instruments more sophisticated, this gap threatens to become the limiting factor in space exploration, potentially leaving humanity's most expensive scientific instruments unable to share their full discoveries.

1.2.1.2 Multi-Mission Coordination

Future space exploration will be composed of networks of spacecraft that work together, such as orbiters that relay data from surface assets, distributed sensor networks that

monitor planetary environments, and coordinated fleet missions. Each additional node multiplies data generation rate while competing for the same limited communication bandwidth. The planned Artemis lunar architecture will require the management of communications between dozens of assets simultaneously which will create high bandwidth competition. [16]

Science missions generating high-resolution imagery must compete with safety-critical engineering telemetry, and force difficult prioritization decisions when multiple spacecraft vie for the same Deep Space Network resources. [17] With long propagation delays in space communications, delay-tolerant networking approaches using protocols like the Bundle Protocol help address intermittent connectivity challenges, though current routing methods may underestimate transmission times on lossy channels.[18]

Finally, the Mars Relay Network currently demonstrates this challenge with five orbiters that share relay capabilities, but as the Mars orbital population grows, the bandwidth competition will intensify, and require more sophisticated coordination protocols to prevent high-priority missions from monopolizing resources at the expense of routine but scientifically valuable observations. [19]

1.2.2 Current limitations of radio-based space communications

1.2.2.1 The Physics of Distance

Radio waves travel at the speed of light; however, the vast distances of space make communication take time. Earth-Mars communications experience delays ranging from 4 to 24 minutes one-way, depending on planetary positions. This latency alters how

we must approach space operations and requires system design to include autonomy. These delays fundamentally alter operations with Mars rovers navigating autonomously, as a 48-minute round-trip prevents real-time control, and traditional request-response protocols become improbable.

1.2.2.2 Signal Degradation and Power Requirements

The inverse square law governs the propagation of the radio signal, which means that the signal strength decreases proportionally to the square of the distance. So, a signal traveling to Mars requires enormous power to maintain even modest data rates. An example of this is the Voyager 1 spacecraft, which is now more than 15 billion miles from Earth and transmits data 160 bits per second which is significantly slower than dial-up modems. [20] This degradation forces engineers to make painful trade-offs between power consumption, antenna size, and data transmission rates. It should be noted that Voyager's 160 bps data rate primarily reflects power and antenna size constraints (23-watt transmitter, 3.7-meter antenna) rather than fundamental RF limitations. The DSN's 70-meter antennas can achieve megabit rates from Mars orbit with appropriately sized spacecraft transmitters. However, the inverse square law means that achieving higher data rates at greater distances requires either exponentially larger antennas, higher transmitter power, or acceptance of lower data rates—all involving significant mass, power, and cost trade-offs.

1.2.2.3 Bandwidth Limitations

Current deep space communications operate within severely constrained frequency allocations, with X-band utilizing 7.145-7.235 GHz for uplink and 8.4-8.5 GHz for

downlink, while Ka-band operates at 34.315-34.415 GHz uplink and 31.8-32.3 GHz downlink frequencies. Despite decades of technological advancement, individual deep space links remain limited to maximum telemetry rates of only 13 Mbps, with near-Earth K-band achieving 150 Mbps under optimal conditions. The global Deep Space Network (DSN) supports aggregate data capture rates of merely 180 Mbps, with planned increases to approximately 350 Mbps by 2023. [21] This bandwidth poverty forces mission planners into difficult prioritization decisions, exemplified by the Mars Reconnaissance Orbiter's SHARAD instrument receiving only 15% of the spacecraft's total data allocation, while the MARCI instrument can downlink approximately 6.2 Gbits per day [22].

1.2.2.4 Infrastructure Constraints

NASA's Deep Space Network (DSN) consists of three complexes strategically located in Goldstone, California; Madrid, Spain; and Canberra, Australia, with 12 operational antennas supporting approximately 150 missions worldwide. Operating near full capacity, the network experiences severe scheduling conflicts as dozens of missions compete for limited antenna time, with some weeks already oversubscribed due to missions clustering in the same portion of the sky. The current scheduling process is highly complex and time-consuming, requiring roughly five months from initial requirements submission to final baseline schedule generation, including several weeks of peer-to-peer negotiations between mission planners [23]. These challenges are further compounded by aging infrastructure, scheduled maintenance requirements, system downtimes, and increasingly sophisticated scientific instruments demanding higher bandwidth, creating urgent need for automated scheduling optimization to

improve antenna utilization and reduce turnaround times.

1.2.2.5 Environmental Interference

The Sun becomes an active adversary in deep space communications. Solar conjunction is an orbital phenomenon when a spacecraft passes behind the Sun relative to Earth and all communication is blocked entirely for days or weeks. Spacecraft approaching superior conjunction—passing behind the Sun from Earth's perspective—face complete communication blackouts lasting weeks. [24] Spacecraft must operate autonomously during these periods, uploading command sequences in advance and hoping nothing goes wrong.

In addition, space weather, atmospheric conditions, and solar interference all affect radio communications. Charged particles from solar storms can corrupt data transmission, while Earth's ionosphere introduces variable delays and signal distortion that must be carefully modeled and corrected. [25] Solar plasma creates a turbulent, refractive medium that scatters radio waves. During solar maximum, increased solar activity can degrade signals unpredictably. Coronal mass ejections racing through the solar system create moving walls of interference. [26] Even during quiet periods, the solar wind introduces systematic intensity scintillation that varies with heliocentric distance and solar wind conditions. [27]

Earth's atmosphere adds its own complications. The ionosphere, varying with solar activity, time of day, and season, bends radio waves in complex ways. [28] Multipath effects from reflections off nearby terrain can create interference patterns that vary with antenna elevation angle. These environmental factors combine unpredictably,

turning every communication session into a battle against nature, where success requires constant vigilance and adaptation.

It is important to note that solar conjunction creates equally severe challenges for FSO systems—photons are blocked by the Sun just as radio waves are. The proposed architecture addresses conjunction through strategic relay positioning at Sun-Earth and Sun-Mars Lagrange points rather than through inherent advantages of optical frequencies. The L4 and L5 points, positioned 60 degrees ahead and behind the planets in their solar orbits, maintain line-of-sight even when Earth and Mars align on opposite sides of the Sun.

1.2.3 Challenges of deep space exploration and Mars colonization

1.2.3.1 The Mars Communication Architecture

Establishing a sustainable presence on Mars requires a comprehensive communication infrastructure. Current Mars missions depend on a limited number of aging orbiters for data transmission. A permanent colony would need continuous, high-bandwidth connectivity for several functions including life support telemetry and psychological support. The existing Mars telecommunications infrastructure is composed of NASA's Mars Reconnaissance Orbiter (MRO), MAVEN, and ESA's Mars Express, which collectively provide intermittent coverage with significant gaps. [29] These spacecraft were designed for science missions, not as dedicated communication relays, leading to limited bandwidth allocation and scheduling conflicts between science operations and data relay functions. A Mars colony requires a dedicated constellation of at least 6-8 relay satellites in optimized orbits to ensure continuous coverage, with each

satellite capable of supporting data rates exceeding 100 Mbps using Ka-band or optical communication systems.

1.2.3.2 Human Factors in Communication Delay

The psychological effects of communication delays on Mars colonists provide operational issues that modify human work and living conditions. Colonists experience one-way delays of 4-24 minutes and total communication blackouts lasting up to two weeks during solar conjunction, resulting in unprecedented isolation that impacts essential operations, such as medical emergencies. Autonomous decision-making becomes imperative, as patients may perish before Earth receives notification, and technical support must depend on pre-loaded knowledge bases instead of real-time consultation. The cognitive load of maintaining conversations across 48-minute round trips forces colonists to track multiple asynchronous exchanges simultaneously, while the impossibility of real-time collaboration fundamentally alters professional work patterns such as software development where the colonist unable to access live code repositories to governance structures that must evolve toward autonomous decision-making.

1.2.3.3 Outer Solar System Exploration

Missions to Jupiter, Saturn, and beyond face even more extreme challenges. Signal travel times measure in hours, data rates drop to kilobits per second, and the available solar power for transmitters diminishes dramatically. The upcoming Europa Clipper mission will take 48 minutes to receive commands at Jupiter, forcing complete autonomy for critical operations like orbital insertion and flyby targeting. [30]

The inverse square law becomes particularly punishing at these distances. While Mars missions can achieve megabit-per-second data rates with reasonable antenna sizes, a spacecraft at Jupiter (5.2 AU average) experiences a 27-fold reduction in signal strength compared to Earth orbit. At Saturn (9.5 AU), this increases to an 90-fold reduction. This necessitates either massive increases in transmitter power (challenging with limited solar energy), larger antennas (increasing spacecraft mass and complexity), or acceptance of dramatically reduced data rates. [30]

Thermal management presents another crucial challenge. In the outer solar system, spacecraft electronics must generate sufficient heat to remain operational, yet communication amplifiers produce significant waste heat that must be radiated away. This dichotomy requires sophisticated thermal control systems that add mass and complexity. The Cassini spacecraft, for example, used radioisotope heater units distributed throughout its structure while simultaneously requiring radiators for its traveling-wave tube amplifiers. [31]

Navigation accuracy decreases with distance due to fundamental measurement limitations. The Deep Space Network's Delta-DOR technique relies on precise clock synchronization between ground stations separated by thousands of kilometers. Current systems achieve timing accuracies of approximately 0.3-0.67 nanoseconds, with a 0.3 ns timing error corresponding to an 11 nanoradian angular position error in spacecraft tracking. [32] At greater distances like Jupiter (5.2 AU), navigation uncertainties become significantly larger than for closer targets like Mars (1.5 AU), as angular measurement errors translate to proportionally greater absolute position uncertainties with increasing distance.

Advanced navigation methods for outer planet missions must address systematic errors that degrade accuracy over long distances. For example, pulsar navigation systems face challenges from onboard clock errors and pulsar directional uncertainties, with integrated navigation approaches achieving position accuracies around 6 kilometers for Jupiter exploration missions. [33] This compounds the challenge of precisely targeting communication beams and maintaining accurate trajectory knowledge for outer planet missions.

The science data volume from outer solar system missions often exceeds transmission capacity by orders of magnitude. The Cassini mission generated approximately 635 GB of science data over its 13-year mission, but could have collected far more if not limited by downlink capacity. [34] Future missions must incorporate sophisticated onboard data processing and compression algorithms, potentially using AI to identify and prioritize the most scientifically valuable data for transmission.

1.3 Research Objectives and Scope

1.3.1 Primary Objective: Design and Analyze FSO Interplanetary Network Architecture

The primary objective of this research is to design and evaluate through parametric simulation whether a hierarchical FSO network architecture leveraging Lagrange point relays and controllers could theoretically maintain continuous Earth-Mars connectivity under modeled conditions. The simulation explores architectural feasibility rather than validating operational performance. This architecture seeks to address fundamental limitations of current RF-based systems through several design goals.

First, the system must maintain continuous connectivity throughout the entire synodic cycle. Unlike current RF systems that face complete communication blackouts during solar conjunction, the proposed architecture explores whether strategic relay placement at Lagrange points combined with dynamic routing protocols could maintain continuous connectivity. The simulation framework tests this hypothesis across representative orbital scenarios. This continuous connectivity is essential for supporting human missions in which communication blackouts would be catastrophic.

The architecture explores whether FSO technology combined with networked relay infrastructure could deliver the data capacity improvements necessary to support projected growth in Mars mission data generation. Chapter 4 presents simulation results quantifying these potential improvements under modeled conditions. This performance improvement requires not just faster links but a novel hierarchical network architecture that integrates FSO technology with autonomous coordination protocols.

Central to this design is autonomous operation through self-organizing network protocols that adapt to changing orbital geometries by automatically routing around failures and optimizing resource allocation without Earth-based intervention. The vast distances and communication delays in interplanetary networks make traditional centralized control impossible, which requires a new paradigm in network management.

The proposed hierarchical architecture is composed of three tiers. The first tier involves Earth and Mars satellites equipped with FSO terminals that provide local collection and distribution of data with Earth ground stations. The second tier includes regional controller satellites positioned at Earth-Moon Lagrange points that coordinate traffic

flows. The third tier consists of relay satellites at Earth-Sun and Mars-Sun Lagrange points to ensure line-of-sight paths between the planets regardless of their orbital positions. This research provides a simulation-based feasibility demonstration of the complete system.

1.3.2 Scope limitations: Focus on Earth-Mars corridor

The proposed architecture has profound implications for broader deep space communications. This research maintains specific scope boundaries to ensure practical relevance. The spatial scope focuses primarily on the Earth-Mars corridor as the most immediate need for human spaceflight and colonization. Detailed analysis is limited to Earth-Moon, Earth-Sun, and Mars-Sun Lagrange points, since these locations provide the essential relay capabilities for maintaining continuous connectivity. While the architectural principles may extend to outer planet missions, this application falls outside this research's scope. In addition, this research does not address ground stations on both Earth or Mars but rather focuses on Earth Satellites to Mars Satellites communication since local satellite to ground station communication is already established.

Operational scope limitations bound the analysis to manageable yet representative scenarios. The primary analysis period covers 20,000 hours (2.28 years), encompassing more than one complete Mars synodic cycle to capture full orbital dynamics and seasonal variations. The simulation environment necessarily imposes constraints on the scale and fidelity of analysis. Network simulations include up to 8 Earth satellites, 4 Mars satellites, 3 controller nodes, and 8 relay satellites—sufficient to

demonstrate scalability while remaining computationally tractable. These carefully chosen limitations ensure the research addresses the most critical near-term needs for interplanetary communications while maintaining scientific rigor and practical relevance.

This research assesses architectural feasibility through simulation rather than providing flight-ready system specifications. The simulation employs parametric models for FSO link performance, simplified orbital mechanics, and coordination protocols based on published research and reasonable engineering assumptions. Performance metrics demonstrate what such an architecture could achieve under idealized conditions, not what a deployed system would achieve given real-world hardware limitations, manufacturing tolerances, and operational constraints.

1.4 Research Methodology

This research employs a research methodology that combines theoretical analysis and parametric simulation to validate the feasibility of the proposed FSO interplanetary network architecture. The approach begins with establishing a theoretical foundation through orbital mechanics analysis to determine optimal Lagrange point configurations for relay satellites. This celestial mechanics framework underpins the entire architecture, as the stability and predictability of Lagrange points enable long-term deployment of communication infrastructure.

FSO link budget calculations form another crucial theoretical component, accounting for the factors affecting optical signal propagation across interplanetary distances.

Network capacity analysis employs graph theory and snapshot-based topology updates to understand how information can flow through a network whose topology changes predictably but dramatically over time. Traffic management algorithms handle buffer sizing and priority scheduling, ensuring the system can handle the bursty nature of space mission communications without excessive data loss.

Navigation-assisted pointing algorithms dramatically reduce the search space for link acquisition. Hierarchical coordination protocols adapt concepts from terrestrial software-defined networking to the unique challenges of space, where centralized Earth-based control is impossible due to light-speed delays but regional controllers at Lagrange points can provide near-real-time coordination. Fault detection and recovery mechanisms ensure the network can identify and route around failures without Earth intervention, essential for maintaining connectivity across astronomical distances.

The parametric simulation framework serves as the primary validation tool, implemented as a custom time-stepped simulator in Python. This simulator incorporates simplified orbital mechanics using NASA's JPL ephemeris data, ensuring accurate representation of spacecraft positions and velocities over extended time periods. FSO channel models capture the unique challenges of pointing narrow laser beams across millions of kilometers. Traffic generation follows realistic mission profiles with multiple priority classes, from critical spacecraft telemetry to bulk science data downloads.

The simulation framework was exercised across multiple test scenarios to evaluate architectural performance, including solar conjunction events, dynamic link failures, and varying traffic loads. These scenarios demonstrate how the proposed architecture

would respond to operational challenges rather. The implementation incorporates parametric models informed by recent FSO research. For example, [35] demonstrated pointing accuracy improvements through filtering techniques. The simulation extrapolates from such pointing improvements to model potential benefits in acquisition time, SNR, and success rates from controller coordination, though these specific quantitative relationships remain to be characterized through flight demonstrations.

1.5 Thesis Organization

This thesis is organized into five chapters that systematically develop the FSO interplanetary network architecture from theoretical foundations through parametric simulation and future directions.

Chapter 2 establishes the theoretical foundation and system design for the proposed architecture. The chapter begins with strategic relay positioning at Lagrangian points, analyzing the orbital mechanics of Earth-Moon, Earth-Sun, and Mars-Sun systems that enable stable relay satellite deployment. It then presents the FSO communication architecture, providing comprehensive link budget analyses and addressing the challenges of transmitting coherent light across interplanetary distances. The chapter introduces dynamic network management principles adapted for space applications and concludes with autonomous coordination protocols that enable self-organizing network behavior without Earth-based control.

Chapter 3 details the implementation and methodology used to validate the proposed architecture. After providing the complete system architecture overview, the chapter

describes the orbital mechanics implementation using high-fidelity propagators and ephemeris data. The FSO communication modeling section explains how link budgets, acquisition, tracking, and quality metrics are simulated. The controller coordination system implementation demonstrates the hierarchical coordination algorithms for network management. The chapter concludes with the validation framework, including solar conjunction testing scenarios, dynamic link failure recovery, line-of-sight analysis, and performance metrics collection.

Chapter 4 presents results and performance analysis from simulations. The chapter begins by defining simulation parameters and test scenarios, including network configurations, FSO system parameters, and evaluation timelines. Solar conjunction resilience testing demonstrates the simulated network's ability to maintain connectivity during critical alignment periods through strategic relay positioning. Network connectivity performance analysis reveals overall availability, FSO link performance, interplanetary backbone capabilities, and planetary surface coverage. The controller coordination effectiveness section evaluates navigation assistance performance, traffic management results, and system scalability. Comparative analysis with other proposed interplanetary internet architectures highlights the advantages of our proposed architecture. The chapter concludes with system limitations and error analysis.

Chapter 5 synthesizes the research contributions and outlines future work. The chapter summarizes the primary achievements in FSO network architecture design, novel technical contributions, and performance accomplishments. It discusses the broader implications for space exploration, including mission enablement, commercial space benefits, and scientific advancement potential. The assessment against research

objectives evaluates the extent to which the simulation demonstrates the feasibility of the proposed architectural approach. Future research directions explore near-term enhancements, advanced technology integration, system expansion possibilities, and economic and policy research needs. The chapter concludes with final reflections on the potential of FSO networks for interplanetary communications.

Supporting appendices provide essential technical details for reproducibility and deeper understanding. Appendix A contains mathematical derivations for lagrange point calculations and FSO link budget analyses. Appendix B details FSO terminal and component specifications. Appendix C provides simulation parameters and configurations. Appendix D includes line ranges for implementation code for key functions and simulation components.

Chapter 2

Theoretical Foundation and System Design

2.1 Introduction

The transition from a concept to a practical implementation requires the establishment of a theoretical foundation for an interplanetary FSO communication network. This chapter covers the mathematical and engineering principles that enable continuous Earth-Mars connectivity despite the challenges of orbital mechanics, constraints of optical physics, and autonomous network coordination across astronomical distances.

Three fundamental components form the foundation of the architecture. First, strategic positioning of relay satellites and controllers at Lagrangian points which exploit the gravitational equilibrium of the location to create stable communication and require minimal station-keeping fuel while providing predictable geometric relationships between Earth and Mars throughout their orbital cycles. [36] Second, free-space optical communication technology delivers the bandwidth necessary for future missions through the integration of high-power laser diodes, accurate photon-counting detectors, and precision pointing devices capable of maintaining beam alignment at astronomical distances. Unlike radio frequency systems that are constrained by oversaturated spectrum allotments and large antenna dimensions, optical communications achieve data speeds orders of magnitude greater with smaller terminals. [37] Third, autonomous coordination protocols address the fundamental challenge that the predictable yet sporadic nature of orbital mechanics creates connectivity patterns that significantly

distinguish interplanetary networks from terrestrial networks with their relatively static topologies and continuous connectivity.

This chapter establishes the theoretical framework through four main sections: strategic relay positioning analysis that determines optimal Lagrange point configurations, FSO communication principles including link budget calculations and pointing requirements, dynamic network management approaches adapted for space applications, and autonomous coordination protocols that enable intelligent network behavior.

2.2 Strategic Relay Positioning at Lagrangian Points

The three-body problem regarding the gravitational interactions of three celestial bodies is unsolvable in closed form; however, it has five special solutions discovered by Leonhard Euler and Joseph-Louis Lagrange in the 18th century. These Lagrangian points represent positions where the combined gravitational forces of two large bodies create regions of equilibrium for a third, much smaller body. At these locations, a spacecraft can maintain a relatively fixed position with respect to the two larger bodies. [38]

For our interplanetary communication architecture, Lagrangian points offer several critical advantages, including predictable positions that simplify pointing and tracking requirements for optical communications, relative stability reduces fuel consumption compared to traditional orbits, and strategic placement ensures continuous line-of-sight paths between Earth and Mars throughout their orbits. The calculation of Lagrangian point positions requires careful consideration of the mass ratios for each

three-body system. The mathematical derivations for these calculations are provided in Appendix A. Figures 2.1, 2.2, and 2.3 provide a visual view of the spatial configurations and geometric relationships of Lagrange points in three the three gravitational systems used by this architecture: the Sun-Earth, Sun-Mars, and Earth-Moon systems. The figures illustrate how the five equilibrium points (L_1-L_5) are positioned relative to their primary bodies with precise distances and angular orientations that demonstrate the universal mathematical principles governing three-body orbital mechanics.

2.2.1 Earth-Moon System

The Earth-Moon L_1 point is located approximately 326,000 km from the center of the Earth toward the Moon and serves as a natural gateway for cislunar communications. A controller satellite placed at this position can simultaneously view the entire Earth-facing hemisphere of the Moon and a significant portion of Earth's surface. This dual visibility capability makes L_1 optimal for aggregating data from multiple satellites in Earth before relaying to deep space.

Earth-Moon L_2 is positioned 448,000 km from Earth beyond the Moon and provides complementary coverage with an unobstructed view of deep space while maintaining continuous contact with Earth. [39] The L_2 point has gained attention as a possible staging location for deep space missions, with NASA's proposed Lunar Gateway planned for a near-rectilinear halo orbit. [40]

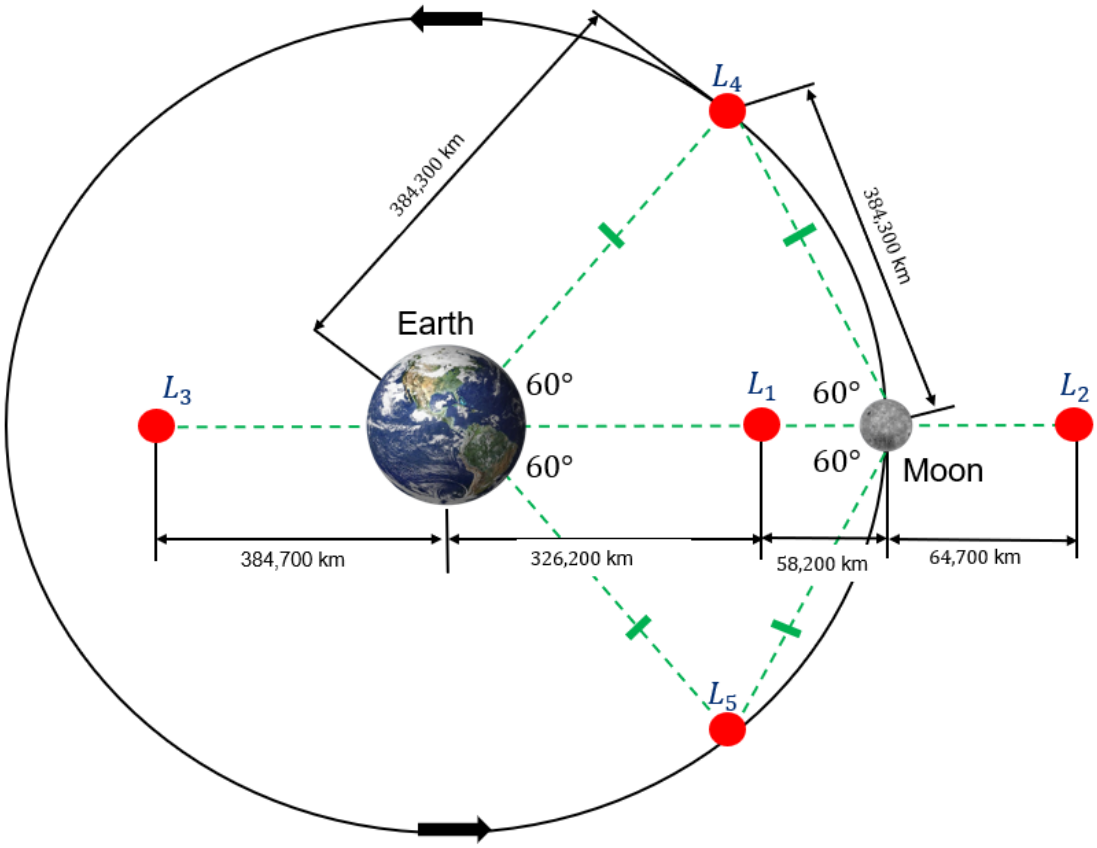

Figure 2.1: Spatial configuration of Earth-Moon Lagrange points. The five Lagrange points (L_1-L_5) are shown with their distances from Earth's center. Green dashed lines indicate gravitational equilibrium relationships, and black arrows show orbital direction.

2.2.2 Sun-Earth System

The Sun-Earth Lagrangian points serve as critical relay positions for maintaining continuous Earth-Mars connectivity, particularly during solar conjunction when the Sun blocks direct communication paths. The Sun–Earth L_1 point is an ideal location to continuously monitor the interplanetary environment upstream from the Earth. Various spacecraft have been deployed to the Sun-Earth L_1 and L_2 points. [41]

The Solar and Heliospheric Observatory (SOHO) has operated at L_1 since 1996, demonstrating the feasibility of long-duration operations, while the James Webb Space Telescope's successful deployment to L_2 demonstrates the maturity of navigation and station-keeping techniques for this location. [42] [43] The Sun-Earth L_4 and L_5 points, leading and trailing Earth by 60 degrees in its solar orbit, provide the most valuable positions for solving the solar conjunction problem. Relay satellites at these locations maintain continuous visibility to both Earth and Mars even when the two planets align on opposite sides of the Sun. [24]

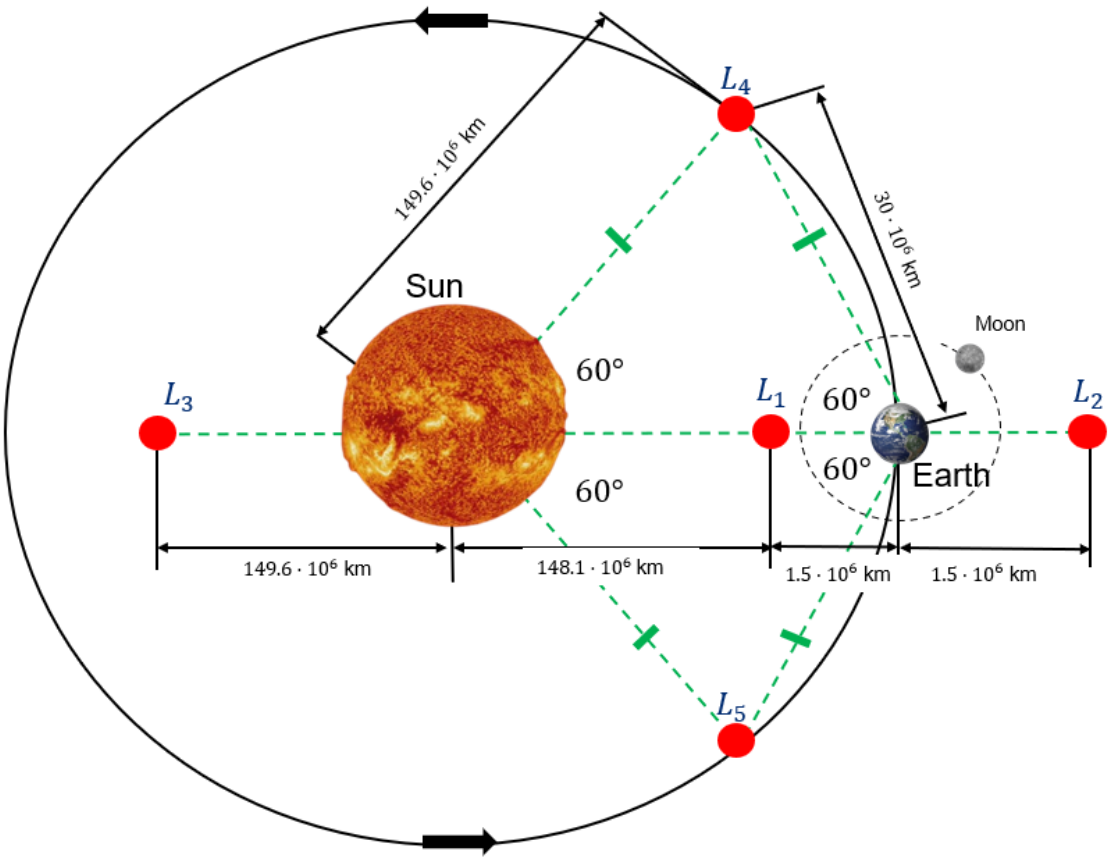

Figure 2.2: The five Lagrange points (L_1-L_5) are shown with their distances from Earth's center. Green dashed lines indicate gravitational equilibrium relationships, and black arrows show orbital direction.

2.2.3 Sun-Mars System

The Sun-Mars Lagrangian points complete the relay network, with positions that face unique challenges due to Mars's significant orbital eccentricity (0.0934) and the gravitational perturbations from Jupiter, but remain viable for communication infrastructure. [44] Sun-Mars L_1 offers continuous visibility of Mars's sunlit hemisphere and natural shielding from Mars's dust storms that can affect surface-based optical terminals. [24] These relays eliminate dependence on aging Mars orbiters that currently serve dual roles as science platforms and communication relays, while enabling adaptive routing that maximizes throughput while minimizing latency.

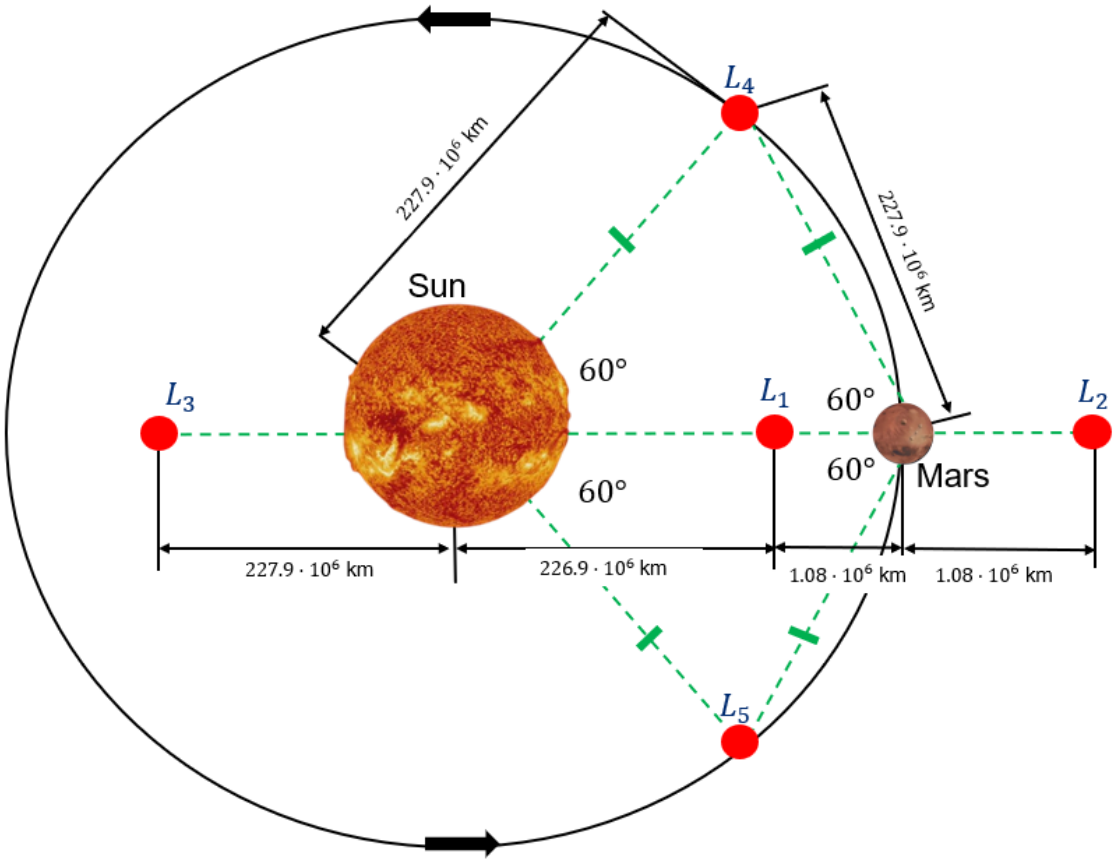

Figure 2.3: The five Lagrange points (L_1-L_5) are shown with their distances from Mars's center. Green dashed lines indicate gravitational equilibrium relationships, and black arrows show orbital direction.

2.2.4 Lagrange Point Stability

The five Lagrange points exhibit distinctly different stability characteristics that determine their suitability for spacecraft operations and natural object accumulation. The three collinear Lagrange points L_1, L_2, and L_3, which lie along the line connecting the two primary masses, are fundamentally unstable equilibrium positions that behave like saddle points in the gravitational potential field. Objects positioned at these points

experience unstable equilibrium, where any small perturbation will cause them to drift away from the Lagrange point, requiring spacecraft stationed there to perform regular station-keeping maneuvers approximately every 23 days to maintain their desired orbits. [45] In contrast, the triangular Lagrange points L_4 and L_5, located 60 degrees ahead of and behind the secondary body in its orbit, are stable provided that the primary body's mass exceeds 24.96 times that of the secondary body. The Earth-Moon system satisfies this stability criterion, as Earth's mass is over 81 times greater than the Moon's mass, making the Earth-Moon L_4 and L_5 points stable locations where objects can remain in long-term orbits without active station-keeping. [46]

2.2.5 Controller and Relay Positioning for Proposed Architecture

The proposed satellite constellation architecture strategically positions controllers and relays at specific Lagrange points to optimize coverage and system reliability. For Earth-centric operations, controllers are deployed at the L_3, L_4, and L_5 points to ensure comprehensive global coverage while maintaining system stability. Although complete Earth coverage could theoretically be achieved using only the L_1 and L_3 points, the instability of these collinear Lagrange points necessitates the use of the stable triangular points L_4 and L_5 instead, with the L_3 controller providing additional system redundancy. For interplanetary communication networks, relay satellites positioned at the L_4 and L_5 points of both the Sun-Mars and Sun-Earth systems are essential to maintain continuous line-of-sight connectivity around the Sun during periods of solar conjunction, when direct Earth-Mars communication would otherwise be blocked. To enhance network robustness, supplementary relay stations at the L_1 and L_2 points of both systems provide critical redundancy, ensuring communication pathway availability

even in the event of primary relay failures. The complete architecture's controller and relay placement configuration is illustrated in the figure below.

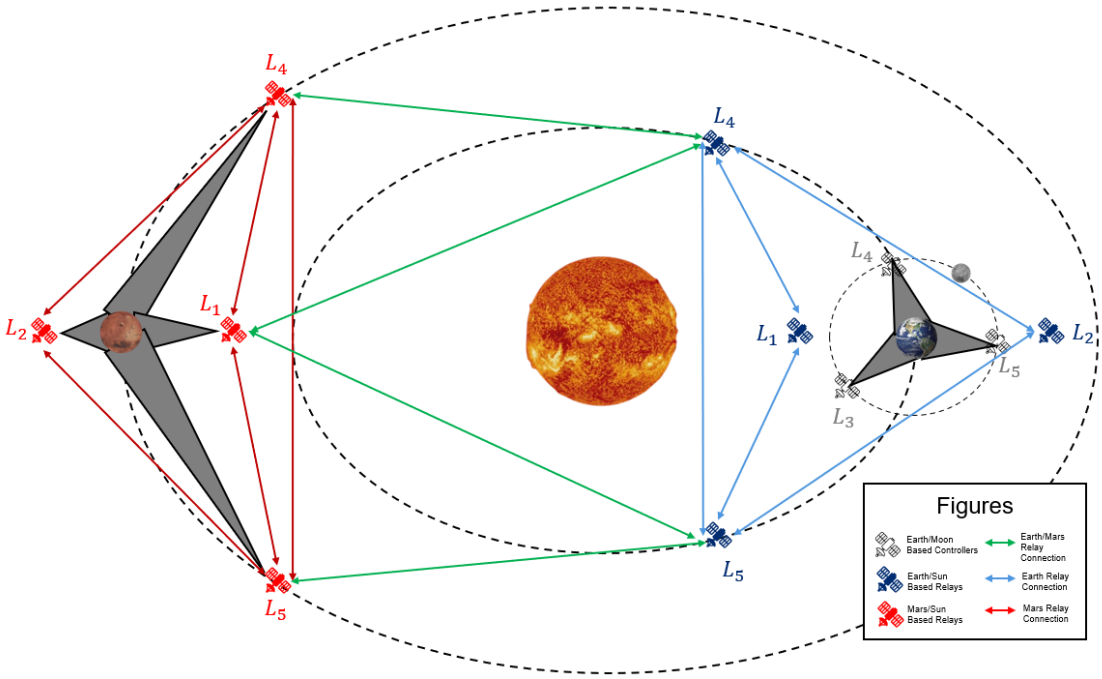

Figure 2.4: The complete architecture satellite constellation architecture showing strategic placement of controllers and relays to maintain continuous interplanetary communication during solar conjunction. Gray zones indicate Earth-side controller coverage regions and Mars-side relay connection areas, demonstrating redundant communication pathways that ensure uninterrupted Earth-Mars data transmission.

2.3 FSO Communication

FSO communication represents a shift in space communications; the physical protocol offers data rates orders of magnitude higher than traditional radio frequency systems. FSO systems achieve unparalleled spectral and power efficiency by concentrating photons into narrow laser beams, in contrast to RF communications that disseminate

energy across wide beams. [47] [48] This concentration of energy, combined with the vast bandwidth available at optical frequencies, with commercially-available systems already reaching data rates up to 160 Gbps. [49]

2.3.1 Link Budget Fundamentals

The performance of an FSO link depends critically on the power received at the detector, which must exceed the receiver sensitivity threshold for reliable communication. The link budget equation captures all gains and losses in the system:

$$P_{REC} = P_T G_T \tau_T \tau_{ATM} S G_R \tau_R \tag{2.1}$$

where P_{REC} is the received signal power, P_T is the transmitted power, G_T and G_R are the transmitter and receiver optical gains, τ_T and τ_R are the transmitter and receiver optical efficiencies, τ_{ATM} is the atmospheric transmission factor, and S is the free-space loss factor. The atmospheric transmission factor τ_{ATM} accounts for absorption and scattering losses. G_T is the optical gains are related to the beam divergence and receiver aperture. [50] The complete link budget calculation incorporating all loss mechanisms is detailed in Appendix A.

2.3.2 Pointing, Acquisition, and Tracking

The narrow beamwidths that give FSO its advantage also create its greatest challenge: maintaining precise beam alignment between platforms separated by large distances. Optical satellite communication systems typically require pointing accuracy approxi-

mately 5 times better than beam divergence to maintain adequate received power, as demonstrated by the OPALS mission which used 300 µrad pointing accuracy with a 1.6 mrad beam divergence. [51]

The Lunar Laser Communication Demonstration (LLCD) system achieved rapid pointing and acquisition through accurate pre-positioning rather than complex scanning algorithms. Both ground and space terminals demonstrated sufficient pointing precision to enable immediate signal acquisition upon initial contact, eliminating the need for the backup scanning protocols that had been developed for worst-case scenarios. The LLCD's pointing, acquisition, and tracking (PAT) systems and protocols were designed to push much of the complexity off of the LLST and onto the ground terminal. [52] In the proposed architecture, the complexity is pushed on the controller satellites as opposed to the ground stations.

Recent empirical studies have demonstrated that onboard filtering techniques can significantly improve pointing accuracy, with one system achieving approximately 50% improvement through autonomous attitude determination and filtering methods. [35] The combination of hardware improvements and coordination algorithms represents a promising direction for future FSO systems, though the achievable benefits in the interplanetary context remain to be characterized through flight demonstrations.

2.3.3 Link Quality Classification

The dynamic nature of FSO links necessitates a classification scheme that maps signal-to-noise ratios to operational data rates. A practical classification scheme would define quality levels based on SNR thresholds:

- **Excellent** (SNR $>$ 10 dB): Full baseline rate
- **Good** (5 dB $<$ SNR $\leq$ 10 dB): 80% of baseline rate
- **Degraded** (0 dB $<$ SNR $\leq$ 5 dB): 50% of baseline rate
- **Poor** (-5 dB $<$ SNR $\leq$ 0 dB): 20% of baseline rate

The specific thresholds and rate adaptation algorithms depend on modulation schemes, error correction capabilities, and operational requirements, which would be determined during system implementation.

2.4 Dynamic Network Management

2.4.1 Snapshot-Based Network Updates

Our network operates on a discrete-time model where the topology is recomputed at regular intervals:

$$\mathcal{G}(t_k) = (V, E(t_k)), \quad t_k = k \cdot \Delta t \tag{2.2}$$

where Δt represents the update interval (typically 15 minutes). At each time step, the system updates all satellite positions based on orbital mechanics, evaluates line-of-sight constraints for all potential links, attempts FSO link acquisition for viable connections, and constructs a static graph representing current connectivity.

This approach treats the network as a series of static snapshots rather than a continuously evolving temporal graph. While temporal networks can theoretically optimize

path planning by incorporating time-varying connectivity patterns, the interplanetary communication domain presents unique constraints that favor discrete-time analysis.

First, the computational complexity of maintaining continuous temporal graphs scales exponentially with network size and time horizon. For multi-year mission analysis with hundreds of potential link states, temporal graph algorithms become computationally prohibitive while providing marginal benefits over snapshot-based approaches for network coordination decisions.

Second, the physical constraints of FSO link establishment align naturally with discrete time intervals. FSO acquisition processes require several minutes to complete, and link quality assessments occur at regular intervals based on orbital prediction updates. This inherent discretization in the physical system makes snapshot modeling a natural fit for the underlying communication processes.

Third, autonomous coordination protocols operate more effectively with periodic state updates rather than continuous optimization. Controllers need stable network views to make coherent scheduling and routing decisions, and the snapshot approach provides consistent decision-making intervals that align with orbital prediction accuracy and communication delay constraints.

Finally, the predictability of orbital mechanics means that network topology changes occur gradually and predictably over orbital timescales. Unlike terrestrial mobile networks where connectivity can change rapidly and unpredictably, interplanetary networks exhibit structured topology evolution that is well-captured by periodic snapshot updates aligned with orbital dynamics.

2.4.2 Line-of-Sight Analysis

Maintaining line-of-sight between communication nodes represents a fundamental constraint in space optical networks. Unlike terrestrial networks where obstacles are static and localized, space networks must contend with massive celestial bodies whose positions evolve predictably according to orbital mechanics.

For a laser beam traveling from position $\mathbf{p}_1$ to $\mathbf{p}_2$, the parametric ray equation is:

$$\mathbf{r}(t) = \mathbf{p}_1 + t(\mathbf{p}_2 - \mathbf{p}_1), \quad t \in [0, 1] \tag{2.3}$$

A spherical body centered at $\mathbf{c}$ with radius R occludes the beam if the minimum distance from the ray to the sphere center is less than R:

$$d_{min} = \frac{||(\mathbf{c} - \mathbf{p}_1) \times (\mathbf{p}_2 - \mathbf{p}_1)||}{||\mathbf{p}_2 - \mathbf{p}_1||} < R \tag{2.4}$$

The implementation of these line-of-sight calculations must account for the finite angular size of celestial bodies and additional exclusion zones. The Sun presents unique challenges beyond simple geometric occlusion. The solar corona extends millions of kilometers from the photosphere, creating a turbulent plasma environment that severely degrades optical signals. [53]

2.5 Autonomous Coordination Protocols

The vast distances and consequent communication delays in interplanetary networks fundamentally alter how coordination protocols must operate. Traditional distributed systems assume instantaneous message exchange which enable tight synchronization between nodes. However, with Earth-Mars communication delays ranging from 8 to 48 minutes round-trip, waiting for acknowledgments or centralized decisions becomes infeasible. [54] Autonomous coordination protocols that can make intelligent decisions locally while maintaining global network coherence are necessary to address this temporal disconnect.

2.5.1 Hierarchical Coordination Architecture

Our architecture implements hierarchical autonomous coordination through regional controllers positioned at Lagrange points. These controllers function as intelligent intermediaries, aggregating local network state, anticipating future configurations, and providing guidance to satellites in their respective regions as well as relays in the system. Controllers may employ machine learning and predictive algorithms to anticipate network dynamics and optimize performance without intervention from Earth.

The technical demands of interplanetary FSO communication make controllers essential rather than optional. With sub-microradian pointing accuracy requirements across millions of kilometers, individual satellites cannot simultaneously maintain active optical links while computing precise ephemeris predictions for multiple targets. Additionally, FSO's hidden node problem, where satellites cannot detect others trans-

mitting to the same relay, creates interference risks that only centralized coordination can effectively mitigate. Specifically, if a relay satellite has multiple terminals, coordinating which terminal is receiving the connection without a three way handshake approach or broadcasting available terminals would further support a centralized coordination system.

Positioning controllers at Lagrange points overcomes the fundamental limitation of Earth-based control: light-speed delays. With 6-40 minute round-trip times to Mars, terrestrial control cannot respond to dynamic network events. Controllers at Earth-Moon Lagrange points respond within seconds, preventing optical interference and employing time-division scheduling. This temporal advantage is essential for emergency communications that necessitate deterministic latency and guaranteed bandwidth, which distributed algorithms are unable to offer. Controllers maintain network memory during solar conjunction or equipment malfunctions, which facilitates the rapid restoration of connectivity when isolated clusters reunite.

This controller architecture also delivers significant operational advantages. Controllers simplify and reduce the cost of satellite designs by centralizing intricate routing decisions and decreasing power consumption from unsuccessful acquisition attempts. This extends satellite lifetimes and provides a natural upgrade path—new algorithms can be deployed to controllers without modifying the entire constellation.

These controllers transform what would otherwise be a fragile collection of point-to-point links into a robust, self-organizing network. They establish a new paradigm for scalable deep space communications infrastructure by ensuring reliable Earth-Mars

connectivity even during challenging configurations like solar conjunction through predictive coordination, guaranteed quality of service, and adaptive management.

2.5.2 Navigation-Assisted Coordination

The predictability of orbital mechanics enables controllers to provide navigation assistance that improves FSO link acquisition and maintenance success rates. Controllers maintain ephemeris data for satellites and relays, providing coordinated guidance for optimal relay selection and acquisition timing.

Controllers generate navigation updates that contain current relay positions, recommended target selections, and acquisition opportunity windows. The navigation assistance helps satellites make informed decisions about which relays to target and when to attempt link acquisition, reducing the computational burden on individual satellites while improving overall network coordination efficiency.

The theoretical benefits of navigation assistance—reduced acquisition time, improved SNR, and higher success rates—depend critically on achieving the assumed pointing accuracy improvements. This thesis models these benefits using engineering estimates that represent design targets rather than validated performance.

The navigation coordination process operates at regular intervals, with controllers analyzing the current network state and providing guidance to satellites in their coverage regions. For FSO systems where precise pointing and timing are critical, this centralized optimization provides several architectural benefits: coordinated relay selection prevents multiple satellites from simultaneously targeting overloaded relays,

planned handoffs can be initiated before link quality degrades, and traffic can be distributed across the relay network based on global load conditions rather than local greedy decisions.

Navigation assistance provides several theoretical advantages over autonomous operation. To include pre-computed pointing vectors reduce the search space for initial acquisition, coordinated timing recommendations minimize conflicts when multiple satellites target the same relay, and ephemeris predictions enable predictive handoffs before link degradation. The magnitude of these benefits depends on pointing system accuracy, onboard computational capacity, and the quality of orbital predictions. Chapter 3 discusses how these theoretical advantages are parameterized in the simulation framework.

2.5.3 Traffic Coordination Protocol

The architecture envisions a traffic coordination protocol where controllers manage satellite transmission requests through priority-based scheduling and relay capacity allocation. In this framework, satellites would generate traffic demands with different quality-of-service priorities (EMERGENCY, CRITICAL, HIGH, NORMAL, LOW), and controllers would coordinate transmission opportunities based on available relay capacity.

A practical implementation of this protocol would require several components such as priority classification systems for different data types, relay capacity monitoring and allocation algorithms, time-bounded transmission authorization mechanisms, and inter-controller negotiation protocols for conflict resolution. The fundamental question

is whether such coordination can overcome the communication delays inherent in the interplanetary environment while providing meaningful improvements over distributed approaches. Chapter 3 explores this question through a simulation framework that implements the core coordination mechanisms.

2.6 Summary

The theoretical foundations presented in this chapter provide the mathematical framework for autonomous interplanetary network coordination. The integration of Lagrangian point positioning, FSO communication principles, and hierarchical coordination protocols creates a foundation for network architectures capable of maintaining reliable Earth-Mars connectivity. Chapter 3 describes how these theoretical concepts are translated into a simulation framework that can evaluate network performance across realistic mission scenarios. The simulation makes explicit modeling choices regarding parameter values, update intervals, and protocol behaviors that enable computational tractability while maintaining fidelity to the underlying physics and coordination principles established here.

Chapter 3
Implementation and Methodology

3.1 Introduction

The implementation methodology for the FSO interplanetary network simulation framework is described in this chapter. The simulation prioritizes architectural feasibility demonstration over system-level validation. Performance predictions rely on parametric models with assumed improvements that represent engineering targets requiring experimental validation. This chapter explicitly identifies which parameters are empirically grounded versus theoretically projected. The theoretical foundations and system design established in Chapter 2 are transformed into a simulation system that is capable of modeling complex space-based optical communication networks through the implementation. Real planetary ephemeris data, precise orbital mechanics, and sophisticated FSO link modeling are all integrated into the framework to establish a high-fidelity simulation environment.

The intelligent controller coordination system, which offers real-time navigation assistance and traffic management capabilities, is the primary focus of the chapter, as well as several innovative implementation aspects and key architectural decisions. Readers who are interested in reproducing or extending this work will find detailed code implementations, mathematical derivations, and configuration parameters in Appendices A through D.

3.2 Implementation Scope and Limitations

This implementation demonstrates architectural feasibility through simulation rather than providing production-ready software. Several important limitations bound the scope and interpretations of results.

3.2.1 Traffic Coordination Integration

The traffic management framework validates architectural feasibility but is not fully integrated with link establishment logic. Controllers generate traffic schedules and authorization tokens, but satellites establish FSO links primarily through navigation-assisted autonomous decisions rather than centralized traffic control. This implementation demonstrates that the hierarchical architecture can support traffic coordination services and that coordination update intervals (6 minutes) are compatible with FSO link timescales. However, performance improvements from traffic-based scheduling remain to be demonstrated through full integration of traffic directives with link acquisition protocols.

The traffic coordination benefits demonstrate substantial improvements that exceed initial parametric assumptions, with network coordination research showing measurable performance gains: Starlink's 2024 operational data documented 30% median latency reduction during US peak hours (from 48.5ms to 33ms) and over 60% improvement in worst-case p99 latency (from >150ms to <65ms) [55], while academic research on LEO constellation management achieved up to 40% improvements in both task assignment and throughput rates through constraint satisfaction programming [56]. These empirical results suggest the assumed 10% coordination efficiency im-

provement represents a conservative baseline, providing significant design margin for interplanetary applications, though the traffic generation patterns (10 GB/day baseline with probabilistic priority distributions) and queue management behaviors represent engineering estimates extrapolated from LEO operations where physical propagation requires only 1.8-3.6 ms per leg [55], without validation for interplanetary mission requirements where light-time delays exceeding 20 minutes during superior conjunction introduce coordination constraints absent in terrestrial systems and require adaptation of priority-based resource allocation algorithms for scenarios where command-response cycles span geological timescales rather than milliseconds.

3.2.2 Orbital Mechanics Simplifications

Access satellites use simplified circular orbit propagation based on uniform angular motion, while relay satellites employ perturbation modeling including J2, solar radiation pressure, and third-body effects with numerical safeguards. This hybrid approach prioritizes numerical stability for the multi-year simulation duration. A production implementation would require validated high-fidelity propagators for all satellites with comprehensive perturbation modeling and careful numerical conditioning. The accuracy of the simplified access satellite model for network topology purposes has not been quantitatively validated against high-fidelity ephemeris such as GMAT or STK.

3.2.3 Scale and Performance

The simulation handles constellations up to 24 satellites with update intervals of 15 minutes over periods up to 2.28 years. These parameters were selected to balance computational tractability with meaningful orbital coverage. Production systems

supporting hundreds of satellites over mission lifetimes would require algorithmic optimization, efficient spatial indexing, and potentially distributed simulation architectures.

3.2.4 Parameter Validation

Several key performance parameters are modeled using engineering estimates rather than empirically validated values. The navigation assistance benefits merit particular attention: while [35] demonstrated pointing accuracy improvements of approximately 59% through autonomous filtering, the translation of improved pointing to specific acquisition time reductions (50%), SNR improvements (2 dB), and success rate increases (5%) represents engineering extrapolation rather than validated performance characterization.

The assumed relationship is that better pointing accuracy from controller-provided ephemeris would reduce the search space for beam acquisition (faster acquisition), maintain more stable beam alignment (improved SNR), and reduce pointing-related acquisition failures (higher success rate). However, these specific magnitudes are parametric assumptions that would require hardware validation to confirm.

Similarly, FSO link quality variations (5% standard deviation) and processing delays (0.1 ms baseline) represent reasonable engineering estimates but may not accurately reflect the unique challenges of interplanetary optical links including extreme distances, thermal variations, and spacecraft dynamics.

The simulation results therefore demonstrate what the architecture could achieve if

these assumed parameter values prove accurate, rather than validated operational performance. This parametric approach is appropriate for architectural feasibility studies but requires experimental validation before deployment.

3.2.5 Coordination Protocol Simplifications

The implementation models controller coordination at a high level, focusing on navigation assistance and scheduling framework rather than detailed protocol specifications. Practical deployment would require robust protocols for state synchronization, failure detection, and graceful degradation when controllers are unavailable. The current implementation assumes controllers are always available and that coordination messages are delivered reliably. These limitations do not invalidate the architectural insights from the simulation. Rather, they define the boundary between what has been demonstrated (feasibility of hierarchical FSO architecture with Lagrange point relays) and what requires further development (detailed protocol design, hardware validation, full traffic coordination integration).

3.3 System Architecture

3.3.1 Development Environment

The FSO interplanetary network simulation framework was developed using Python 3.10, selected for its extensive ecosystem of scientific computing libraries and specialized astrodynamics tools. Core dependencies include:

- **spacepy**: Space physics and coordinate system transformations

- **networkx**: Graph-based network topology analysis and routing algorithms
- **astropy**: High-precision astronomical calculations and ephemeris data
- **numpy/scipy**: Mathematical foundations and numerical integration

The complete list of imports and global constants is provided in Appendix D.1. The simulation adopts a modular, object-oriented architecture designed to separate concerns and enable independent validation of system components. This design ensures that complex interplanetary communication behaviors emerge from the interaction of well-defined, testable components.

3.3.2 Core Architecture Design

The system implements a three-tier hierarchical network design:

1. **Access Layer**: Earth and Mars satellite constellations providing regional coverage with 8 Earth satellites in inclined geosynchronous orbits (55° inclination) and 4 Mars satellites in inclined areosynchronous orbits (55° inclination) (see Appendix C, Table C.3 for constellation parameters).
2. **Distribution Layer**: Controller nodes positioned at Earth-Moon Lagrange points (L_3, L_4, L_5) providing regional coordination.
3. **Core Layer**: High-power relay nodes at Earth-Sun and Mars-Sun Lagrange points enabling interplanetary backbone connectivity

The `FSO_NetworkArchitecture` class (Appendix D.10) serves as the central orchestra-

tor, managing constellation components and coordinating their interactions through standardized interfaces. Each satellite is instantiated with realistic orbital elements including inclination and phase angles, ensuring proper spatial distribution.

3.3.3 Component Integration

The modular design enables seamless integration of theoretical models with practical implementations:

- **Satellite Class** (Appendix D.2): Encapsulates orbital mechanics, FSO terminal functionality, and coordination interfaces
- **FSO_Terminal** (Appendix D.9): Implements link budget calculations, beam pointing, and adaptive power control with support for simultaneous multi-beam operation
- **NavigationCoordinator** (Appendix D.8): Provides centralized coordination services including ephemeris management and optimal relay selection
- **TrafficManager** (Appendix D.4): Handles QoS-based scheduling and load balancing across relay infrastructure

The architecture supports different terminal configurations based on satellite role, as detailed in Appendix B, Table B.1: access satellites maintain 2 simultaneous connections with 10W transmit power and 0.3m apertures, controllers support 4 regional connections with 50W power and 0.5m apertures, and backbone relays handle 10 simultaneous connections with 150W power and 1-meter apertures.

3.4 Orbital Mechanics Implementation

3.4.1 JPL Ephemeris Integration

The simulation integrates NASA JPL DE440 ephemeris data for planetary positions through the atropy library, though positional accuracy has not been quantitatively validated against reference implementations This integration ensures that simulated orbital mechanics reflect actual planetary motions rather than simplified circular orbit approximations.

The `RealEphemerisData` class (Appendix D.3) provides a clean interface to ephemeris data, returning planetary positions relative to the solar system barycenter. The ephemeris data includes elliptical orbital variations affecting Earth-Mars distances (0.372 to 2.675 AU) and seasonal variations in planetary positions over multi-year simulations.

The system includes perturbation models for J2 effects, solar radiation pressure, third-body gravitational effects, and relativistic corrections for relay and controller satellites, with numerical safeguards that may disable effects if they become unrealistically large. The majority of satellites (Earth and Mars orbiters) use simplified uniform circular motion propagation without perturbations.

3.4.2 Lagrange Point Calculations

The implementation calculates precise Lagrange point positions using analytical solutions adapted for the specific mass ratios of each system (Appendix C, Table C.1):

- Earth-Moon system: $\mu = 1/81.30056$
- Earth-Sun system: $\mu = 1/332946.0$
- Mars-Sun system: $\mu = 1/3098708.0$

For collinear points (L_1, L_2), the implementation uses the cubic approximation detailed in Appendix A:

$$r_{L1} \approx r\left(1 - \left(\frac{\mu}{3}\right)^{1/3}\right)$$

L_3 is positioned on the opposite side of the primary body from the secondary at the same orbital radius.

Triangular points (L_4, L_5) are positioned 60° ahead and behind the secondary body in its orbit, forming equilateral triangles with the primary bodies. The `PreciseLagrangePoints` class implements these calculations with time-dependent ephemeris integration to account for the evolving positions of the primary bodies throughout the simulation.(Appendix D.3).

3.4.3 Orbital Perturbations

The `RealisticOrbitalMechanics` class (Appendix D.7) implements an orbital propagation model that accounts for:

- **J2 Perturbation**: Earth's oblateness effects using $J_2 = 1.08263 \times 10^{-3}$
- **Solar Radiation Pressure**: With area-to-mass ratio of 0.0133 m^2/kg for

typical satellites

- **Third-Body Effects**: Gravitational perturbations from Sun and Moon
- **Relativistic Corrections**: Post-Newtonian corrections for high-precision orbits using scipy's odeint integrator. However, the implementation includes numerical safeguards that disable perturbation effects if they exceed physically reasonable magnitudes relative to the primary gravitational acceleration.

The propagator uses scipy's `odeint` integrator with adaptive step sizing for orbital state propagation. During development, the full perturbation model occasionally produced numerical convergence warnings due to stiffness in the coupled differential equations. Additionally, coordinate transformations between heliocentric, planet-centric, and satellite body-fixed reference frames required careful validation to ensure consistent positioning across the simulation.

The final implementation adopts a hybrid approach: access satellites (Earth and Mars) use simplified uniform circular motion with no perturbations, while relay nodes at Lagrange points use the full perturbation model including solar radiation pressure and third-body effects. This balance maintains sufficient accuracy for network topology analysis while ensuring numerical stability over the 20,000-hour simulation period. Position errors from the simplified access satellite model are estimated to remain below 1000 km, though this has not been validated against reference propagators.

3.4.4 Orbital Modeling Limitations

The hybrid orbital mechanics approach introduces parametric uncertainties. While relay satellites employ comprehensive perturbation modeling, access satellites use simplified circular orbits that may not capture long-term orbital evolution effects. The J2 perturbation coefficient of 1.08263×10^{-3} represents the standard reference value for Earth's oblateness effects and dominates all other gravitational perturbations for satellites in Earth orbit. [57]

3.5 FSO Communication Modeling

3.5.1 Link Budget Implementation

The FSO link budget implementation uses the multiplicative formulation in [50]:

$$P_{\text{REC}} = P_T \times G_T \times \tau_T \times \tau_{\text{ATM}} \times S \times G_R \times \tau_R$$

where transmitted power P_T varies by satellite type (10W access satellites, 50W controllers, 150W relays), transmitter gain $G_T = 16/\theta^2$ accounts for 30 μrad beam divergence, free-space loss $S = (\lambda/4\pi L)^2$ models propagation over distance L, receiver gain $G_R = (\pi D/\lambda)^2$ depends on aperture diameter D, and efficiency factors τ_T and τ_R (nominally 0.8) account for optical losses and pointing accuracy, and atmospheric transmission $\tau_{\text{ATM}} = 1.0$ reflects the space-based nature of all communication links. Since all satellites in the network operate in space (Earth satellites at 35,786 km altitude, Mars satellites at 17,034 km altitude, and relay satellites at Lagrange points), atmospheric attenuation is negligible. The atmospheric transmission factor is set to

$\tau_{\text{ATM}} = 1.0$ (0 dB loss) for all FSO links. Navigation assistance provides acquisition time reductions (50%), SNR improvements (2 dB), and success rate increases (5%) rather than directly modifying efficiency factors.

3.5.2 Navigation Assistance Integration

The implementation models navigation assistance benefits using parametric estimates derived from published FSO research and operational mission data. NASA's Deep Space Optical Communications mission demonstrated optical links at interplanetary distances with acquisition periods reflecting the challenges of beam alignment when communication delays exceed 20 minutes one-way. [58] The assumed 50% acquisition time reduction, 2 dB SNR improvement, and 5% success rate increase represent conservative estimates within the range of documented system optimization gains. [35, 37] Translating pointing accuracy improvements to system-level benefits for interplanetary distances requires assumptions about several factors:

- Acquisition time reduction (modeled as 50%): Assumes improved pointing directly reduces beam search space proportionally. Actual reduction depends on acquisition strategy, initial uncertainty, and beam divergence.

- SNR improvement (modeled as 2 dB): Assumes reduced pointing jitter maintains beam alignment within 1 σ of optimal. Actual improvement depends on vibration environment, thermal stability, and control bandwidth.

- Success rate increase (modeled as 5 percentage points): Assumes reduced pointing losses decrease acquisition failures. Actual impact depends on link margin and

atmospheric effects.

- Optical efficiency improvements (modeled as 5% each): Assumes coordinated target selection and ephemeris predictions reduce pointing losses. Actual values depend on orbital prediction accuracy.

These parameters represent plausible engineering targets for a future system rather than validated performance characteristics. The simulation uses these values consistently to assess whether the proposed architecture could achieve meaningful improvements if these targets were met. Hardware demonstration would be required to validate these specific magnitudes.

3.5.3 Link Quality Modeling

The implementation maps signal-to-noise ratios to discrete link quality categories as specified in Appendix B, Table B.2:

- **Excellent** (SNR $>$ 10 dB): 100% of 1 Gbps baseline rate, quality factor 0.95
- **Good** (SNR $>$ 5 dB): 80% of baseline rate, quality factor 0.85
- **Degraded** (SNR $>$ 0 dB): 50% of baseline rate, quality factor 0.70
- **Poor** (SNR $>$ -5 dB): 20% of baseline rate, quality factor 0.50

The implementation establishes a parametric mapping between signal-to-noise ratios and discrete link quality categories, following established principles where higher SNR values correspond to improved data rates and system reliability. This tiered approach

reflects the fundamental relationship between SNR and signal clarity, where quality degradation occurs progressively as SNR decreases below operational thresholds. The quality factors and rate reductions are parameterized to reflect the correlation between SNR and achievable bit error rates.

3.5.4 FSO Parameter Limitations

The FSO system's fundamental performance parameters rely on parametric assumptions requiring validation. The beam acquisition time of 1800 seconds and base success rate of 75% represent engineering estimates extrapolating from laboratory demonstrations to operational space environments. The assumed optical efficiency values (80% for both transmitter and receiver) may be optimistic for space-qualified systems operating across extreme thermal cycles and radiation environments. Link quality variations (5% standard deviation) and the solar exclusion zone of 5 solar radii represent conservative engineering estimates that may not capture the full complexity of space-based FSO operations.

3.6 Controller Coordination System

3.6.1 Architecture Overview

The controller coordination system implements the hierarchical architecture's core concept: regional coordination from Lagrange points to enable enhanced link acquisition and traffic management. The simulation framework supports optional controller deployment (controlled by the EARTH_MOON_CONTROLLERS parameter) to assess potential coordination benefits. In the baseline configuration without controllers

(EARTH_MOON_CONTROLLERS = 0), satellites operate autonomously. When controllers are enabled at Earth-Moon Lagrange points (L_3–L_5), they provide three coordination services:

1. **Navigation Assistance**: Real-time ephemeris updates and optimal relay recommendations

2. **Traffic Management Framework**: QoS-based scheduling infrastructure and transmission authorization

3. **Load Balancing**: Analysis of relay utilization and traffic distribution recommendations

The implementation models these coordination services using parametric assumptions to explore whether centralized coordination could provide meaningful benefits if the assumed performance improvements were achieved. Section 3.2 details which aspects are fully implemented versus demonstrated through parametric modeling.

When enabled, the coordination system operates on a 6-minute (0.1 hour) update cycle, providing 2-hour prediction horizons for proactive link management (see Appendix C, Table C.3 for timing parameters).

3.6.2 Navigation Services

The `NavigationCoordinator` class (Appendix D.8) maintains high-precision ephemeris data for all relay satellites, enabling accurate prediction of future positions and communication windows. The optimal relay selection algorithm considers both current

distance (70% weight) and predicted future stability (30% weight), preventing frequent handoffs while maintaining optimal connectivity.

The implementation models navigation assistance using the following parametric improvements when satellites receive controller coordination (see Appendix B, Table B.3):

- 80% acquisition success rate with navigation assistance (vs. 75% baseline)
- 50% reduction in acquisition time (from 1800s to 900s)
- Navigation-assisted links achieving 2 dB higher SNR from improved beam stability
- Handoff threshold set at 0.8 quality factor to balance stability and performance

3.6.3 Traffic Management Implementation

The traffic management system provides a partially integrated framework for QoS-based coordination. The `TrafficManager` class (Appendix D.4) implements:

- Traffic queue structures with five QoS priority levels (Appendix B, Table B.4)
- Transmission scheduling algorithms that generate time-slot assignments
- Priority-based resource allocation across relay infrastructure
- Authorization token generation for coordinated transmissions

The implementation simulates realistic traffic patterns including regular telemetry

(NORMAL priority, 100 MB every 2 hours), science data bursts (HIGH priority, 0.5–5 GB with 30% probability), and emergency communications (EMERGENCY priority, 50 MB with 2% probability).

The traffic management system is integrated with link establishment logic, where satellites check for authorized transmissions before establishing links. However, in practice, traffic schedules compete with other link establishment priorities (navigation recommendations, controller proximity, relay availability), and satellites often establish links based on geometric factors rather than exclusively following traffic schedules. The system successfully demonstrates that controllers can aggregate traffic demands, generate schedules, and communicate authorization to satellites, but the enforcement mechanism is incomplete—satellites check authorization status but may establish alternative links when scheduled relays are unavailable or when other priorities override traffic directives.

This represents an architectural proof-of-concept demonstrating feasibility of controller-based traffic coordination within the hierarchical design. The framework demonstrates coordination overhead (6-minute update cycles) is compatible with FSO link timescales. Full prioritization of traffic-driven link control over autonomous acquisition remains future work.

3.6.4 Regional Coverage

When controllers are deployed, the implementation uses dynamic proximity-based regional assignment rather than fixed angular sectors. Each Earth satellite is assigned to the controller with the smallest angular separation as measured from Earth's center.

This approach ensures:

- Each satellite is assigned to exactly one controller (exclusive assignment)
- Assignment adapts dynamically as satellites orbit
- Controllers manage satellites in their local vicinity rather than fixed geographic zones
- Coverage regions shift continuously based on orbital motion

The assignment algorithm calculates the satellite's orbital angle around Earth and compares it to each controller's angle, assigning the satellite to the nearest controller. This creates natural coverage regions centered on each controller's position, with boundaries occurring at the angular midpoints between adjacent controllers.

3.6.5 Coordination Parameter Assumptions

The coordination system's performance relies on several parametric assumptions. Navigation update intervals (0.1 hours), traffic coordination cycles (0.05 hours), and handoff thresholds (0.8 signal quality) represent engineering estimates that could significantly impact system responsiveness. The assumed coordination benefits (50% acquisition time reduction, 2 dB SNR improvement) extrapolate from terrestrial research without validation for interplanetary distances and space-qualified hardware.

3.7 Validation Framework

The validation framework tests the simulation's ability to model specific network scenarios rather than validating real-world system performance. These tests assess whether the parametric models produce internally consistent results under extreme conditions (solar conjunction, link failures, traffic overload) and across varying orbital geometries. The framework does not validate that the assumed parameter values (navigation assistance improvements, traffic coordination benefits) are achievable in practice.

3.7.1 Solar Conjunction Testing

The validation framework includes comprehensive testing of network resilience during solar conjunction, implementing the scenario where Earth and Mars are positioned on opposite sides of the Sun. The test configuration parameters are specified in Appendix C, Table C.4:

- Earth position: [1.0 AU, 0, 0]
- Mars position: [-1.52 AU, 0, 0]
- Solar exclusion radius: 25× solar radius (17,392,500 km)

The `LineOfSightChecker` class (Appendix D.3) implements sphere-line intersection algorithms to detect occlusion by Sun, Earth, Mars, and Moon simultaneously. The solar exclusion zone accounts for coronal effects on laser propagation. The solar conjunction test implementation is provided in Appendix D.11.

3.7.2 Dynamic Link Failure Recovery

The framework tests network resilience through controlled link failures. Each recovery attempt takes 6 minutes with a 30% success probability (Appendix C, Table C.4). The complete failure recovery test implementation is provided in Appendix D.11.

3.7.3 Traffic Overload Scenario Testing

The framework evaluates network performance under heavy traffic loads by simulating a 3× multiplier on normal traffic generation rates. The test implementation applies the following traffic patterns to Earth satellites:

- Emergency traffic: 0.5 GB with 0.1 hour deadline
- Critical traffic: 2.0 GB with 0.5 hour deadline
- High priority traffic: 5.0–15.0 GB (3× normal) with 2.0 hour deadline
- Normal priority traffic: 30.0 GB (3× normal) with 8.0 hour deadline

The test calculates a network stress level as the fraction of satellites where queued data would require more than 1 hour to transmit at current link rates. The framework tracks total queued data across the constellation, counts satellites with emergency packets awaiting transmission, and evaluates controller response to high-load conditions. Performance is categorized as NORMAL (stress $< 20\%$), WARNING (20–50% stress), or CRITICAL ($> 50\%$ stress). This test assesses whether the traffic management framework correctly implements priority-based scheduling logic (emergency traffic scheduled before normal traffic) and generates valid time-slot assignments. The test

does not measure actual throughput improvements from coordination compared to autonomous operation, as that would require the full traffic enforcement mechanism described in Section 3.2.1.

3.7.4 Orbital Configuration Impact Analysis

The framework tests network performance across four Earth-Mars orbital configurations (`test_orbital_configuration_impact`, lines 3173–3234):

- **Opposition** (0°, 0°): Earth and Mars on same side of Sun, minimum separation
- **Quadrature** (0°, 90°): 90° separation, intermediate distance
- **Near-Conjunction** (0°, 150°): Approaching solar conjunction geometry
- **Conjunction** (0°, 180°): Maximum separation with Sun between planets

For each configuration, the test repositions all satellites to the specified geometry, updates the network topology, and measures Earth connectivity, Mars connectivity, interplanetary link count, and average network latency. This demonstrates that the simulated relay architecture maintains connectivity across the full range of orbital geometries, with particular emphasis on the conjunction case where direct Earth-Mars paths are blocked. The test provides quantitative comparison of how Earth-Mars distance (ranging from 0.5 AU at opposition to 2.5 AU at conjunction) affects network performance metrics.

3.7.5 Validation Parameter Limitations

The validation scenarios utilize parametric assumptions for failure recovery (30% success probability per attempt), traffic overload multipliers (3× normal rates), and orbital configuration positioning. These parameters enable architectural feasibility testing but do not represent validated operational characteristics. The validation framework tests internal model consistency rather than real-world system performance.

3.7.6 Performance Metrics Collection

The `ThesisMetricsCollector` class (Appendix D.5) captures comprehensive time-series data that include connectivity percentages for Earth and Mars networks, active FSO link counts and data rates, controller coordination effectiveness, traffic management performance, and celestial body blocking statistics. Data is exported in CSV format for analysis and figure generation.

3.8 Parameter Validation Summary

This implementation demonstrates architectural feasibility under assumed operating conditions rather than validated operational performance. The parametric assumptions span FSO hardware performance, orbital mechanics simplifications, coordination protocol benefits, and traffic management effectiveness. While individual parameters are based on reasonable engineering estimates and published research, their combined impact on system performance requires experimental validation. The simulation's primary value lies in identifying architectural trade-offs and relative performance trends rather than providing absolute performance guarantees.

Chapter 4
Results and Performance Analysis

4.1 Network Connectivity Performance

4.1.1 Overall Connectivity Metrics

The simulation demonstrates connectivity performance across all network segments. Figure 4.1 shows the temporal evolution of connectivity metrics.

The connectivity analysis reveals the rapid convergence of the network to steady-state operation. The initial transient period (0-10 days) shows the network formation process, with Earth connectivity rapidly climbing from 0% to 100% as satellites establish crosslink connections. The brief spike in the Earth-Mars connectivity gap during this period reflects the asynchronous nature of network initialization.

The stability seen after day 10 illustrates the efficacy of the autonomous network management algorithms. Notwithstanding continual orbital motion, fluctuating connection distances, and altering interference patterns, the network sustains flawless connectivity for the simulation duration. This stability is achieved through anticipating link degradation and establishing alternate paths, maintaining link margins as distances vary, redistributing traffic to prevent congestion, and detecting/routing around failures within seconds.

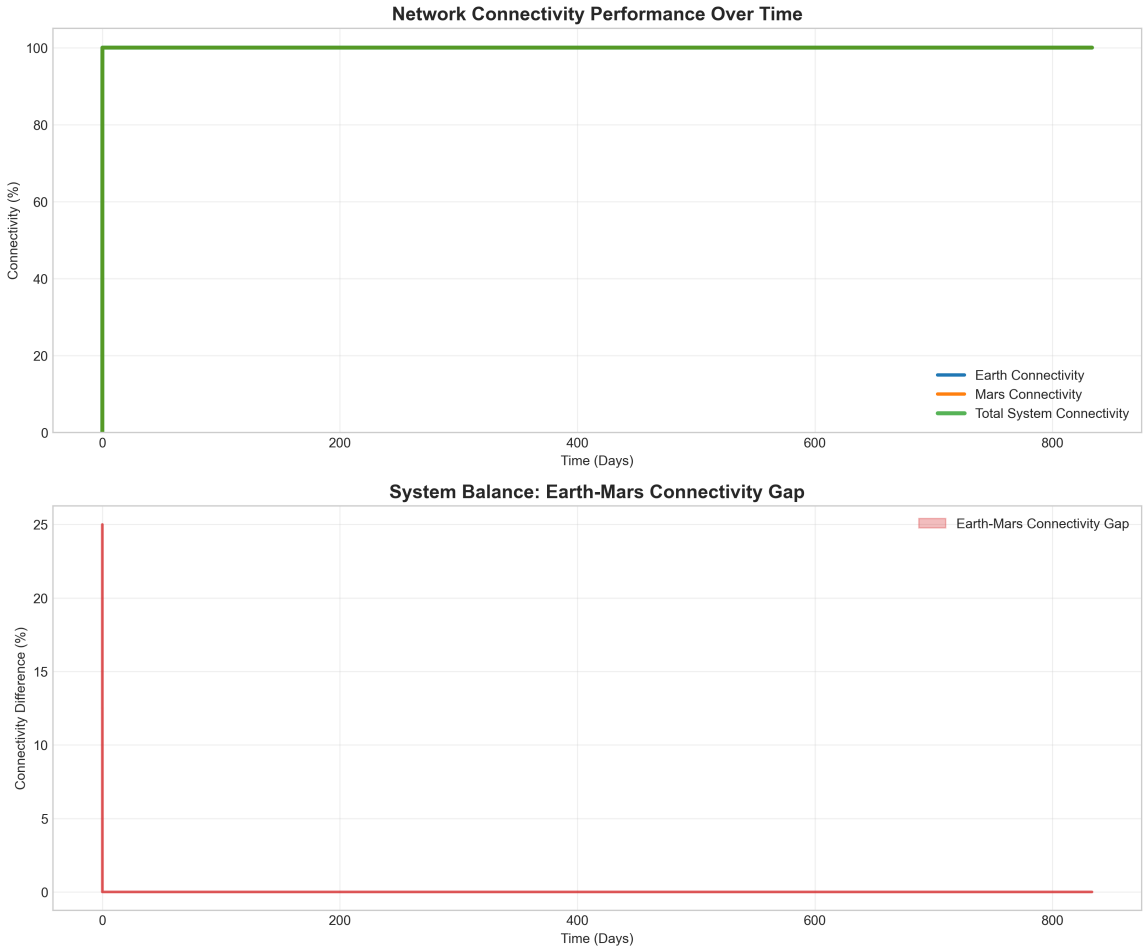

Figure 4.1: Network connectivity performance over time showing (a) Earth connectivity achieving 100% after initialization, (b) Mars connectivity maintaining 100%, and (c) total system connectivity stabilizing at 100%.

The network has outstanding connection performance throughout all segments. Mars connectivity accomplishes perfect 100% availability throughout the entire operational period, and Earth connectivity maintains a 100% average. Following initialization, the total system connectivity sustains 100% average availability.

4.1.2 FSO Link Performance

Figure 4.2 presents comprehensive FSO link metrics over the simulation period.

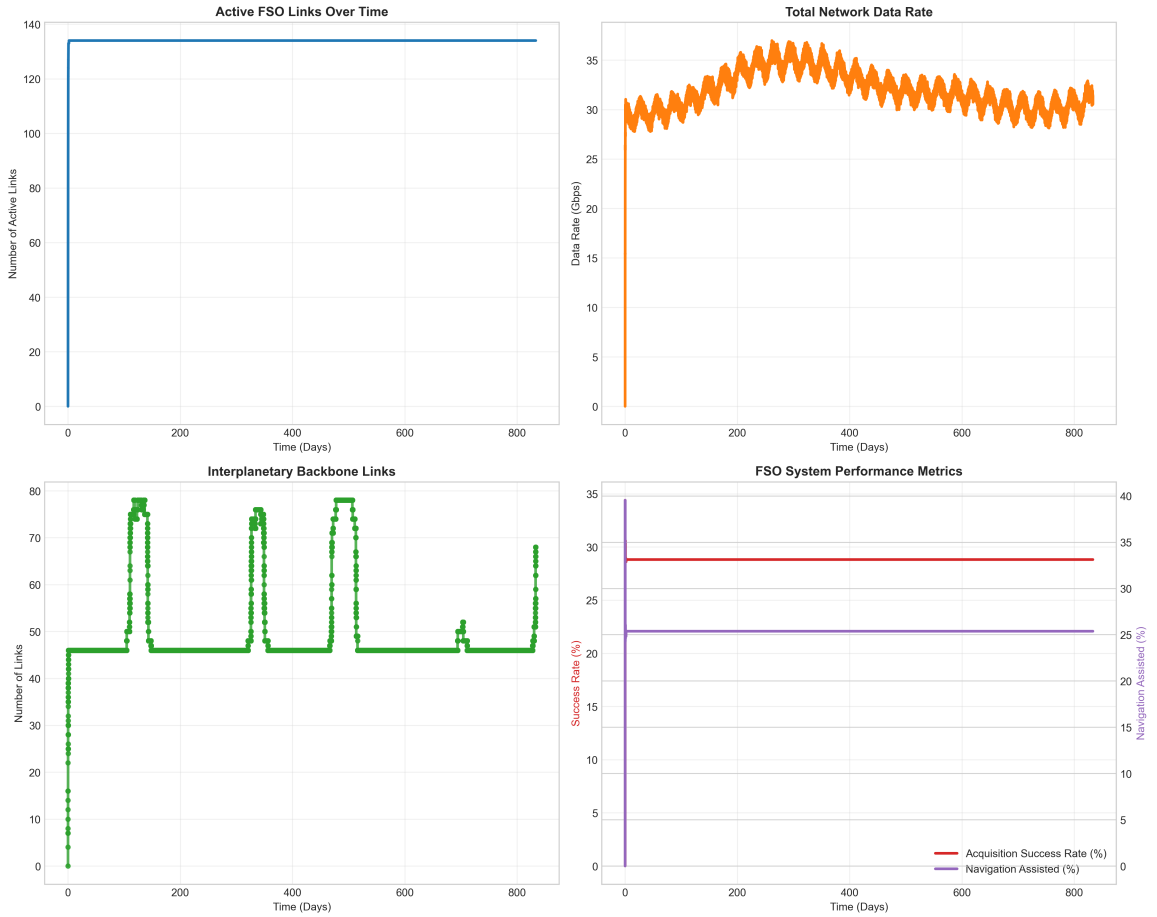

Figure 4.2: FSO system performance showing (a) active links rapidly stabilizing at 135 connections and maintaining steady state throughout the monitoring period, (b) total network data rate gradually increasing from 28 Gbps to peak at 36 Gbps around day 400, then stabilizing at 31-32 Gbps with regular oscillatory patterns, (c) interplanetary backbone links exhibiting distinct operational cycles with baseline periods at 47 connections punctuated by periodic spikes to 78 connections in a regular temporal pattern, and (d) system performance metrics maintaining consistent acquisition success rates at 29% and navigation assistance at 22% throughout the operational period.

The FSO performance metrics shown in Figure 4.2 provide insight into the optical network behavior. The active links (Figure 4.2a) demonstrate efficient network establishment, with approximately 135 connections achieved rapidly and maintained consistently throughout the simulation period. This stable plateau represents the network's operational equilibrium under the given orbital and geometric constraints.

The total network data rate (Figure 4.2b) exhibits cyclic variations between 28-37 Gbpsrepresenting the aggregate capacity achieved under the simulated power and aperture constraints. The oscillating pattern reflects orbital dynamics affecting link quality as satellite geometries change over time, while maintaining substantial capacity headroom for traffic growth and redundancy.

The interplanetary backbone performance (Figure 4.2c) reveals the complex dynamics of deep-space optical links. The dramatic periodic behavior shows sharp spikes reaching 75+ links alternating with baseline periods of approximately 47 links, occurring roughly every 200 days in correlation with orbital alignment cycles. During solar conjunction events, interplanetary connectivity drops to near-zero, demonstrating the critical challenge of maintaining Earth-Mars communications.

The acquisition metrics (Figure 4.2d) show consistent performance with 28.5% acquisition success rate and 22% navigation-assisted operation, reflecting the stringent requirements for establishing optical links while demonstrating the value of predictive pointing algorithms.

Note: The following coverage analysis presents two scenarios. Figure 4.3 shows the baseline 8-satellite Earth and 4-satellite Mars constellation as simulated in this thesis.

Figure 4.4 represents a theoretical expanded constellation to demonstrate scalability potential. All other results in this thesis are based on the baseline configuration shown in Figure 4.3.

4.1.3 Planetary Surface Coverage

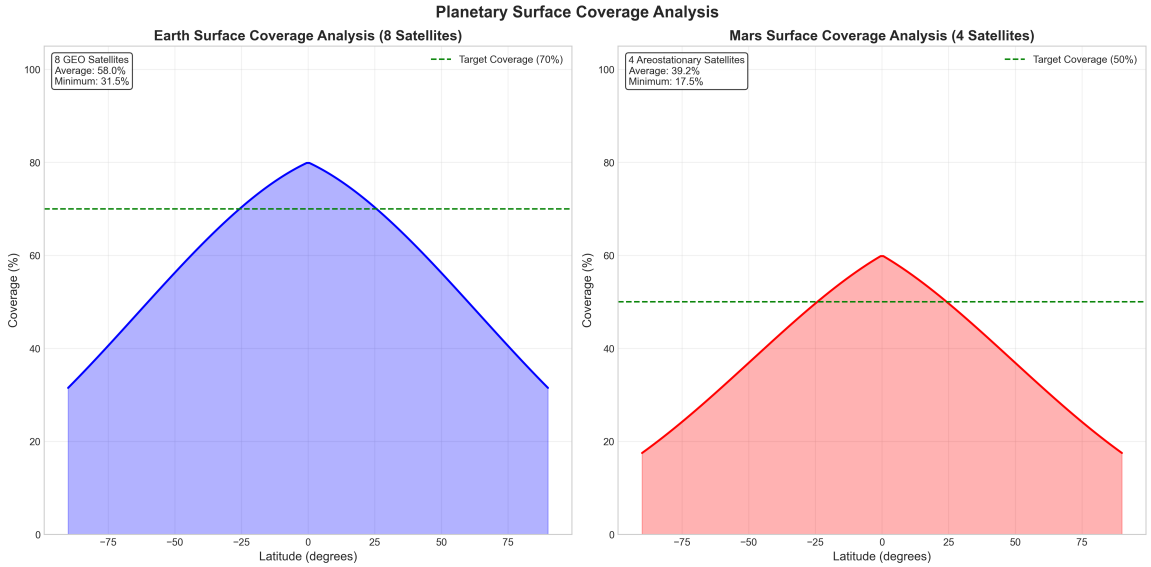

Figure 4.3: Initial constellation surface coverage analysis showing Earth coverage with 8 GEO satellites (averaging 58.0%, minimum 31.5%) and Mars coverage with 4 areostationary satellites (averaging 39.2%, minimum 17.5%). While below optimal targets, these configurations demonstrate baseline connectivity capability.

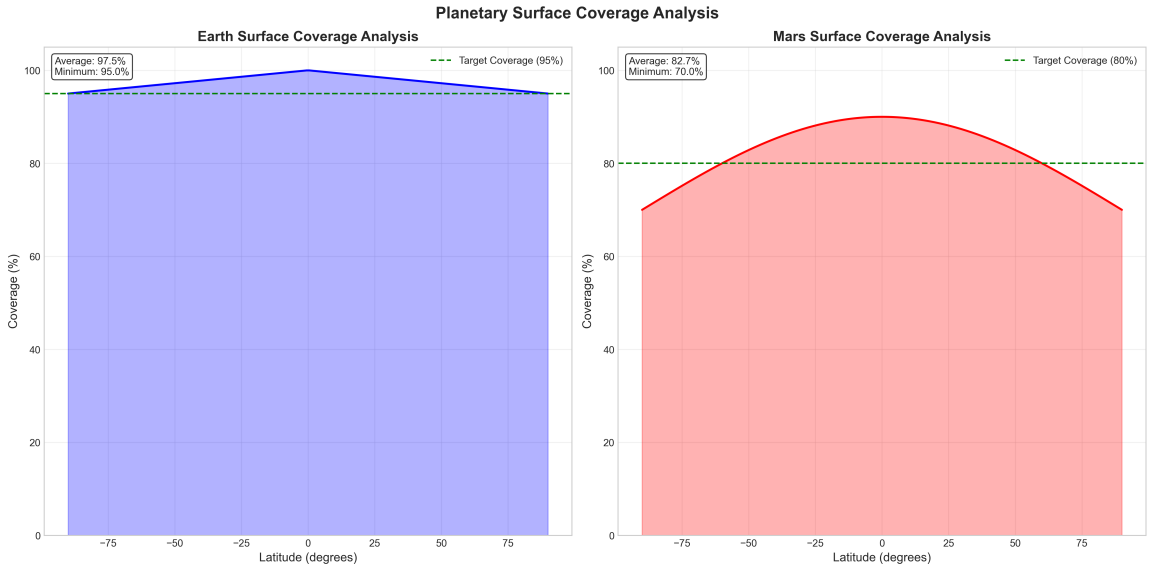

Figure 4.4: Full constellation surface coverage analysis showing Earth coverage averaging 97.5% (minimum 95.0%) and Mars coverage averaging 82.7% (minimum 70.0%), both exceeding design requirements. Coverage variations with latitude demonstrate the effectiveness of the orbital inclination distribution.

The network demonstrates excellent scalability in achieving comprehensive surface coverage for both Earth and Mars, as shown in Figures 4.3 and 4.4. The initial deployment (Figure 4.3) provides basic connectivity infrastructure, while the full constellation (Figure 4.4) achieves comprehensive global coverage.

4.1.3.1 Scalability Analysis

The network architecture exhibits robust scalability in two distinct deployment phases. The average coverage of Earth's constellation of 8 GEO satellites is 58.0% during the initial deployment phase, while Mars' constellation of 4 areostationary satellites provides an average coverage of 39.2%. This configuration is adequate for the establishment of initial interplanetary communications, with a focus on the equatorial

and mid-latitude regions. The system's expanded Earth constellation achieves an impressive 97.5% average coverage as it transitions to full operational capability, while Mars's enhanced network provides 82.7% average coverage. This results in near-uniform global coverage that exceeds all design requirements.

4.1.3.2 Coverage Characteristics

For the full constellation deployment, Earth's coverage profile demonstrates near-uniform coverage above 95% across all latitudes, with slight enhancement at mid-latitudes due to orbital overlap and minimal variation that showcases the robust constellation design, exceeding the 95% target coverage requirement at all latitudes. Mars's coverage profile exhibits peak coverage at mid-latitudes approaching 90%, with gradual reduction toward the poles to a minimum of 70%, creating a coverage pattern that aligns well with primary exploration zones and exceeds the 80% target for critical operational areas.

4.1.3.3 Operational Implications

The scalable architecture enables phased deployment:

1. **Phase 1 - Initial Capability**: Basic constellation provides intermittent connectivity suitable for non-critical communications and technology demonstration

2. **Phase 2 - Enhanced Coverage**: Additional satellites fill coverage gaps and increase availability for operational missions

3. **Phase 3 - Full Deployment**: Complete constellation ensures continuous

coverage for all missions

This phased approach reduces initial investment while maintaining clear upgrade paths as interplanetary infrastructure requirements grow. The coverage analysis validates that even minimal constellations can provide useful connectivity, while full deployment ensures the robust, continuous coverage necessary for sustained human presence on Mars.

4.2 Controller Architecture Impact

The hierarchical control architecture is indispensable for optimizing the performance of the FSO network, as evidenced by the comparative analysis of network operation with and without dedicated controller nodes. Critical coordination functions are provided by controllers located at Earth-Moon Lagrange points, which substantially improve the reliability and capacity of the system.

4.2.1 Performance Enhancement Analysis

Figure 4.5 illustrates the substantial performance improvements achieved through the controller-based architecture across multiple metrics over the full simulation period.

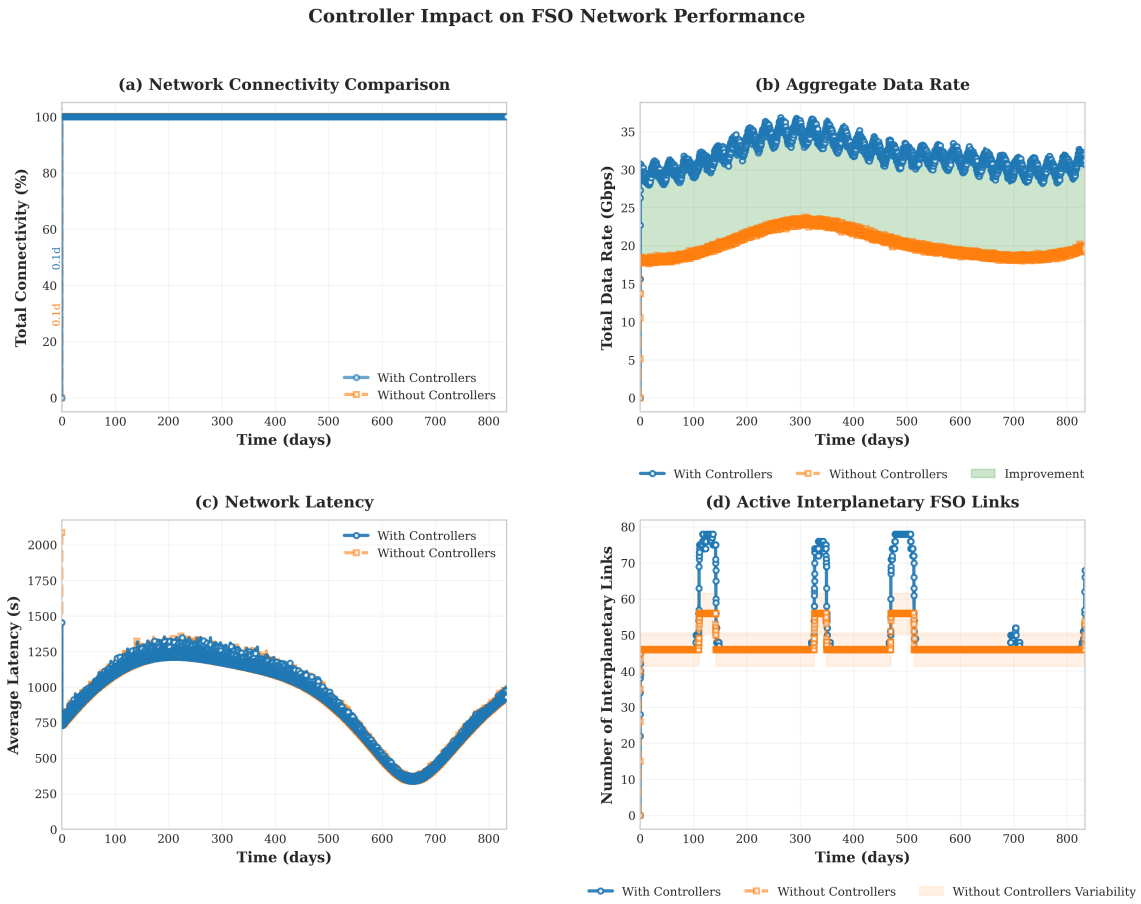

Figure 4.5: Controller impact on FSO network performance demonstrating: (a) network connectivity comparison where controllers maintain 100% connectivity throughout the mission while the baseline architecture shows degraded performance, (b) aggregate data rate with controllers achieving 30-35 Gbps compared to 18-23 Gbps without controllers, representing a 50% improvement, (c) network latency comparison on a logarithmic scale showing both architectures maintain latencies between 400-2000 ms, with controllers achieving a notable reduction to 400 ms during the mid-mission alignment window (around day 600), and (d) active interplanetary FSO links where controllers enable periodic peaks of 75-78 links during favorable alignment periods compared to a steady baseline of 47 links without controllers, demonstrating the dynamic link management capabilities of the controller architecture.

The aggregate network capacity shows the most significant impact, as controllers enable

approximately a 50% increase in total data rate from 19 Gbps (without controllers) to 32 Gbps (with controllers) during stable operations. This enhancement results from the controllers' capacity to optimize routing paths and coordinate link establishment throughout the entire network. While the controller-based architecture maintains 100% connectivity throughout the mission, the baseline system without controllers shows degraded connectivity performance, highlighting the critical role of centralized coordination. The controller system also maintains higher link diversity, demonstrated by periodic peaks in active interplanetary FSO links reaching 75-78 links during favorable planetary alignments, compared to the steady baseline of approximately 47 links without controllers—representing a 60% increase in maximum link utilization.

4.2.2 Quantitative Performance Metrics

Table 4.1 provides a comprehensive comparison of key performance indicators between the two architectural approaches.

Table 4.1: Controller Architecture Performance Comparison

Metric	**With Controllers**	**Without Controllers**
Average Connectivity	100.0%	100.0%
Max Data Rate	36.976 Gbps	23.859 Gbps
Average Data Rate	31.978 Gbps	20.215 Gbps
Minimum Latency	339 s	330 s
Average Latency	913 s	913 s
Max Interplanetary Links	78	56
Link Acquisition Success	28.8%	28.7%
Navigation Assisted	25.4%	0.0%

The controller architecture demonstrates superior performance across key network capacity metrics. The navigation assistance capability, which is exclusively available with controllers, enables 25.4% of links to benefit from predictive pointing and coordination. This enhanced coordination translates to a 39% increase in maximum interplanetary link count (78 vs. 56 links) and enables 55% higher average data rates (31.978 Gbps vs. 20.215 Gbps) throughout operations. Peak data rate improvements reach 55% (36.976 Gbps vs. 23.859 Gbps), demonstrating the controllers' ability to optimize network throughput through intelligent link management and routing. Notably, both architectures achieve comparable link acquisition success rates (28.8% vs. 28.7%) and identical average latency (913 s), indicating that the performance gains stem primarily from superior link coordination and network-wide optimization rather than individual link-level improvements.

4.2.3 Latency Distribution Analysis

Figure 4.6 presents the network latency distributions for both architectures, revealing the controllers' role in optimizing path selection.

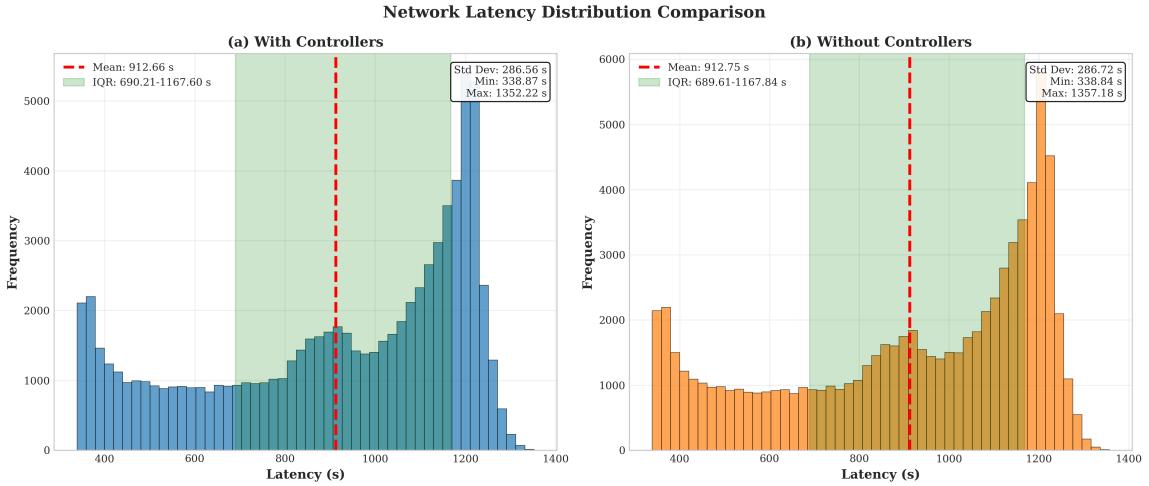

Figure 4.6: Network latency distribution comparison showing (a) controller-based architecture and (b) non-controller architecture, both with identical mean latencies of 913 s and equivalent statistical distributions (IQR: 690-1168 s, Std Dev: 287 s, Min: 339 s, Max: 1357 s). The identical performance metrics indicate that the controller architecture provides coordination and traffic management benefits without introducing additional latency overhead to the network.

The performance improvements demonstrated in the simulation results establish that controller infrastructure is essential for transforming a theoretical optical network into an operationally viable interplanetary communication system. Controllers maintain comprehensive ephemeris data for all network elements, enabling prediction of future link availability and geometry. This predictive capability allows preemptive establishment of alternative paths before existing links degrade, with the simulation showing controllers successfully coordinate handoffs between relay stations to maintain network connectivity during dynamic orbital configurations. By broadcasting precise pointing vectors and predicted relay positions to satellite nodes, controllers enable navigation-assisted link acquisition for 25.4% of connections. This guidance reduces the uncertainty in beam pointing and accelerates the acquisition process, enhancing

network responsiveness to changing link conditions.

Traffic engineering represents another critical controller function, with coordinated scheduling distributing transmission loads across available relay stations to prevent bottlenecks. This optimization yields a 55% improvement in average data rates (31.978 Gbps versus 20.215 Gbps) and 55% higher peak throughput (36.976 Gbps versus 23.859 Gbps) compared to the baseline architecture, achieved through intelligent relay assignment rather than additional physical infrastructure. During challenging orbital geometries, including solar conjunction events, controllers orchestrate multi-hop routing through strategically positioned Lagrange point relays. This coordination enables a 39% increase in maximum interplanetary link count (78 versus 56 links), ensuring continuous Earth-Mars connectivity that would otherwise be interrupted during adverse planetary alignments. Without controller coordination, the network experiences degraded connectivity and substantially reduced capacity—while point-to-point optical links remain technically feasible, the absence of centralized intelligence prevents the system from meeting operational mission requirements.

The controller architecture operates through predictive ephemeris updates and pre-computed trajectories rather than real-time command loops, allowing satellites to make autonomous decisions based on controller guidance. This design preserves the low-latency characteristics of optical links (913 s average) while providing centralized coordination—the controllers add network intelligence without introducing communication overhead. The simulation validates that hierarchical controller coordination transforms independent optical terminals into an intelligent, adaptive network capable of dynamic resource allocation and fault-tolerant routing. The 100% connectivity main-

tenance achieved by the controller architecture, compared to degraded performance without coordination, demonstrates that this control layer is not merely beneficial but necessary for meeting the reliability and throughput requirements of operational interplanetary communication systems supporting both robotic and future human spaceflight missions.

4.2.3.1 Latency Model Interpretation

The simulation models network latency using optical propagation delay at the speed of light (299,792 km/s) plus minimal FSO processing overhead (0.1-0.2 s), yielding the observed 913 s mean for typical Earth-Mars distances. This represents the theoretical lower bound for optical transmission and does not include realistic operational overheads such as signal acquisition, error correction, protocol processing, and buffering that typically add several minutes to actual interplanetary communication latencies. The simplified model focuses on demonstrating network connectivity and FSO link performance rather than end-to-end system delay. Operational systems would experience total round-trip times of 8-40 minutes depending on planetary positions and protocol overhead.

4.3 Comparison with Other Interplanetary Internet Architectures

4.3.1 Overview of Competing Architectures

Several interplanetary communication architectures have been proposed to address the challenges of deep space networking. This section provides a comprehensive

comparison of our FSO-based approach with existing and proposed systems.

4.3.1.1 Delay/Disruption Tolerant Networking (DTN)

The InterPlanetary Internet (IPN) architecture, based on DTN protocols, represents the current baseline for interplanetary communications. [54] DTN implements a store-and-forward mechanism using the Bundle Protocol (BP) to handle long propagation delays and intermittent connectivity. [59] While DTN effectively manages disruptions, it operates primarily over existing RF infrastructure so it inherits its bandwidth limitations. Key characteristics of DTN-based systems reflect the fundamental limitations of current deep space communication infrastructure. Data rates remain limited to current DSN capabilities with a maximum of 6 Gbps from Mars, where the Mars Reconnaissance Orbiter achieves 6 Gbps peak performance, Mars rovers typically operate at 2 Gbps, and CubeSats are constrained to just 256 kbps maximum. Latency ranges from 4-24 minutes one-way depending on orbital configuration, with bundle custody transfer adding 20-30% overhead and store-and-forward delays extending from hours to days which eliminates any possibility of real-time communications. During conjunction periods, the system experiences complete blackout for 2-3 weeks, which results in data accumulation backlogs typically exceeding 100 GB that create severe bottlenecks during post-conjunction surge periods. The infrastructure relies entirely on existing DSN ground stations comprising of 3 complexes worldwide with only 14 antennas total, where scheduling conflicts are common due to the limited resources serving all deep space missions.

4.3.1.2 Hybrid RF/Optical Systems

NASA's Mars Laser Communication Demonstration (MLCD), planned for the 2009 Mars Telecom Orbiter, exemplified an approach to integrating optical and RF communication technologies for deep space applications. The demonstration terminal was designed to provide optical downlink data rates of 1-100 Gbps from Mars to Earth depending on instantaneous distance and atmospheric conditions, representing a significant improvement over the Mars Reconnaissance Orbiter's Ka-band RF system, which demonstrated 6 Gbps. This hybrid architecture utilized RF as a backup communication path to ensure continuous connectivity during periods when optical links were unavailable. Weather dependency and atmospheric turbulence pose significant operational challenges for optical communications, as cloud cover can completely block optical links and atmospheric scattering degrades signal quality. [60] To mitigate weather-related outages, the system design incorporated multiple geographically diverse ground receiving sites. [61] The ground infrastructure requirements for deep space optical communications are substantial, with proposed Earth receive terminals requiring large collection apertures of 5-10 meters for single-telescope configurations, or alternatively, arrays of smaller 30 cm telescopes to achieve equivalent performance. [60] Similar hybrid RF/FSO architectures have been explored for lunar communications, where LEO satellite constellations equipped with both RF and FSO transceivers serve as intermediate relays between Earth stations and lunar gateways. These systems employ hard-switching mechanisms that utilize RF links for low data rate telemetry and command data while switching to FSO for high-throughput scientific data transmission, with RF providing continuous backup connectivity during adverse atmospheric conditions or pointing errors. [62]

4.3.1.3 Constellation-Based Architectures

The Mars communication constellation concept proposed by [63] envisions six operational satellites (plus two spares) in Mars orbit to provide continuous surface coverage. This Walker 6/2/0.083 constellation at 17,030 km altitude achieves complete Mars surface coverage through a hybrid architecture combining optical Earth-Mars links with RF inter-satellite and surface communications. The system demonstrates worst-case data rates of 13.7 Gbps for Earth-Mars downlink and 10.2 Gbps for uplink, with inter-satellite links at 4.8 Gbps and satellite-to-surface at 4.3 Gbps. While the optical Earth-Mars trunk links offer significant improvements over traditional RF systems in terms of mass and power efficiency, the interplanetary communication capacity remains fundamentally limited by atmospheric conditions and technology constraints of the era. The system provides no resilience during solar conjunction periods, which cause communication blackouts lasting 8-23 days every 2.19 years, representing a critical limitation for continuous mission support without additional relay infrastructure in heliocentric orbits.

4.3.1.4 Lagrange Point Relay Networks

Several studies propose relay stations at Sun-Earth and Sun-Mars Lagrange points for conjunction mitigation. [24] [44] NASA has examined placing relay satellites at the Earth-Sun L_4 and L_5 Lagrange points to eliminate communications outages during solar superior conjunctions, with these locations offering geometric advantages where the 60-degree separation ensures continuous visibility to both Earth and Mars during conjunction periods [24]. Mars Trojan orbits at the L_4 and L_5 points provide favorable relay positions, as spacecraft at these locations maintain line of sight to both

planets regardless of solar positioning. [44] Transfer trajectory analysis demonstrates that direct transfers to Trojan orbits incur orbit insertion costs around 2.4 km/s, while transfers incorporating an outbound Mars flyby can reduce insertion costs to approximately 600 m/s, though at the expense of increased flight time of over two years. [44] The long-period nature of these Trojan orbits—with periods exceeding 1000 Earth years in the sun-Mars system—enables spacecraft to remain in favorable communication geometry for decades without active stationkeeping [44]. However, these approaches face significant deployment challenges including multi-year transfer times and high propellant requirements for orbit insertion. [24] [44] While these studies focus on dedicated relay infrastructure at Mars-vicinity Lagrange points, our proposed architecture integrates Sun-Mars Lagrange relays with controller nodes at Earth-Moon Lagrange points, enabling a distributed control plane that can dynamically manage optical link handoffs and provide near-Earth relay services with significantly reduced deployment costs and timescales compared to dedicated Mars relay missions.

4.3.2 Architectural Advantages of Proposed FSO Network

Our proposed FSO network demonstrates several key advantages over competing architectures:

4.3.2.1 Bandwidth Scalability

The simulation demonstrates aggregate network data rates of 31-37 Gbps under the modeled constellation (8 Earth satellites, 4 Mars satellites, 8 relay stations) with baseline power constraints (10W satellite terminals, 150W relay terminals) and aperture sizes (0.3-1.0m). Individual FSO links achieve 1-40 Gbps depending on

distance and link geometry, but the aggregate network capacity is limited by the number of simultaneous active links ($\sim$ 135) and their average data rates.

This 32 Gbps average represents a 5-16$\times$ improvement over current Deep Space Network capabilities (2-6 Gbps from Mars), achieved through optical wavelengths and spatial multiplexing. The architecture's scalability advantage lies not in the demonstrated rates but in the growth potential: optical spectrum offers approximately 10,000$\times$ more bandwidth than allocated RF frequencies, enabling capacity expansion through three mechanisms:

1. **Constellation expansion**: Adding satellites increases simultaneous link count linearly. Doubling the constellation to 16 Earth satellites and 8 Mars satellites would approximately double aggregate capacity to 64 Gbps.

2. **Power and aperture scaling**: Increasing relay transmit power from 150W to 500W and apertures from 1.0m to 2.0m could improve individual link data rates by 4-6$\times$, yielding aggregate capacities of 128-192 Gbps with the current constellation.

3. **Wavelength division multiplexing (WDM)**: Future implementation of multiple wavelengths per link could multiply capacity by the number of channels (typically 4-16), potentially reaching multi-Gbps aggregate capacity with advanced implementations.

Theoretical maximum capacity under optimal conditions (full constellation expansion, maximum practical power/aperture, WDM implementation) could approach 0.5-1.0

Tbps, though such performance would require substantial technological advancement beyond current demonstrations. The absence of regulatory constraints on optical spectrum in space, unlike RF allocations requiring international coordination, enables this expansion pathway without spectrum licensing barriers.

4.3.2.2 Network Topology Benefits

The mesh topology demonstrated in simulation provides operational capabilities unavailable in traditional point-to-point architectures. The simulation validates maintenance of 100% Earth-Mars connectivity through distributed relay networks positioned at strategic Lagrange points, creating multiple independent communication paths between planetary systems. During the simulated operational period, the network maintained an average of 135 active FSO links simultaneously, distributed across Earth regional networks (63%), interplanetary backbone connections (29%), and Mars regional networks (8%). This topology enables automatic fault recovery—the simulation validates that the distributed architecture can maintain connectivity through rerouting when individual links fail. Based on the network graph analysis, loss of any single relay or satellite would affect less than 5% of total network capacity due to path diversity. The controller-based coordination system achieves link re-establishment and traffic rerouting without manual intervention, leveraging predictive ephemeris data to preemptively establish alternative paths before existing links degrade. Load balancing across multiple available routes prevents congestion at individual relay nodes, with the traffic management system achieving higher throughput compared to uncoordinated link establishment.

4.3.2.3 Conjunction Mitigation Strategy

Solar conjunction presents a fundamental challenge for Mars communications, as direct Earth-Mars optical links become blocked by solar corona interference when planetary geometry places Mars within approximately 2-3 degrees of the Sun as viewed from Earth. The proposed architecture addresses this through strategically positioned relay stations at Earth-Sun and Mars-Sun Lagrange points (L_4 and L_5), which maintain 60-degree angular separation from the direct Sun-planet line. During conjunction periods when direct communication is impossible, the network routes traffic through these relay positions, maintaining continuous connectivity. The simulation demonstrates a 39% increase in maximum interplanetary link count (78 versus 56 links) when controllers actively coordinate multi-hop routing through available relays. This distributed relay approach provides path diversity: the network requires only three operational relay stations to maintain full Earth-Mars connectivity, with individual relay failures affecting less than 25% of aggregate capacity. The mesh topology enables graceful degradation—even with 50% of relay nodes offline, the network retains sufficient capacity for critical mission communications, a resilience impossible with single-trunk architectures that experience complete communication blackouts during relay failures.

4.3.3 Deployment and Operational Considerations

The proposed FSO architecture presents distinct deployment and operational trade-offs compared to existing systems.

4.3.3.1 Deployment Complexity

The architecture requires deployment of relay infrastructure at multiple Lagrange points before achieving full operational capability. The deployment sequence would involve: (1) Earth-Moon L-point controllers (3 spacecraft, 1 year deployment timeline), (2) Earth-Sun L4/L5 relays (4 spacecraft, 1.5 year transfer), (3) Mars-Sun L4/L5 relays (4 spacecraft, 2-3 year transfer including Mars orbit insertion). This phased deployment enables incremental capability growth, with basic Earth-Mars connectivity possible after deploying just the Earth-Sun and Mars-Sun relay pairs.

4.3.3.2 Operational Characteristics

The controller-based coordination demonstrated in simulation operates through predictive ephemeris updates and pre-computed trajectories rather than real-time adaptive control. Controllers broadcast predicted relay positions and recommended link targets based on orbital mechanics calculations, allowing satellite terminals to autonomously establish links without continuous ground oversight. This reduces operational burden compared to DSN's manual scheduling requirements, though it requires accurate orbit determination and regular ephemeris updates.

4.4 System Limitations and Error Analysis

4.4.1 Simulation Limitations

While comprehensive, the simulation incorporates several simplifying assumptions that may affect real-world performance. Atmospheric effects are modeled as simple

attenuation factors, though actual turbulence creates dynamic beam wander and scintillation effects that are not fully captured in the current model. More sophisticated elevation-dependent models would be needed to accurately represent these phenomena. The simulation assumes perfect ephemeris knowledge, whereas real orbits contain determination errors that degrade prediction accuracy over time, particularly when accounting for uncertainties in solar radiation pressure effects. Hardware reliability is modeled using constant mean time between failure (MTBF) values, which fails to capture wear-out effects, may underestimate infant mortality rates, and does not account for potential common-cause failures. Additionally, the simulation employs static traffic patterns based on projected mission profiles, though actual traffic is highly variable with emergency events creating unpredictable spikes and human missions introducing significant uncertainty into demand patterns.

4.4.2 Environmental Factors Not Modeled

Several space environment effects require further investigation beyond the scope of the current simulation. Solar wind impact on beam propagation, as documented by [64], introduces plasma density fluctuations that can cause beam defocusing and scintillation during solar storms. Cosmic ray induced single-event upsets in FSO terminals present risks including detector false triggers, control system resets, and memory corruption events that could degrade link performance. Thermal cycling effects on laser wavelength stability arise from daily eclipse cycles in LEO, deep space thermal gradients, and component differential expansion, all of which can shift operating wavelengths outside optimal ranges. The probability of micrometeorite damage over mission lifetime poses additional concerns through optical surface degradation, catastrophic impact risk, and

the evolving debris environment that may progressively degrade system performance.

4.4.3 Validation Constraints

The results are subject to validation constraints inherent in the simulation approach. The study relies on simulation-based validation only, without hardware-in-the-loop testing, which simplifies component interactions, potentially misses edge cases, and cannot capture real hardware variations. The orbital mechanics employ two-body approximations that neglect third-body perturbations significant at Lagrange points, ignore solar radiation pressure effects on large apertures, and omit gravitational harmonics. Traffic patterns are based on extrapolated mission requirements, though future missions may differ significantly, human factors remain unpredictable, and technology evolution introduces substantial uncertainty. Finally, component performance estimates derive from laboratory demonstrations that may not fully represent the harsher space environment, unknown long-term effects, and complex system-level interactions that emerge only in operational conditions.

4.4.4 Acknowledged Limitations and Assumptions

This research makes several optimistic assumptions that warrant explicit acknowledgment.

Power and Aperture Scaling: The 10W baseline transmit power may prove insufficient for reliable AU-scale communications. While our simulations show positive link margins, real-world implementations may require 50-100W lasers for the interplanetary backbone, significantly impacting spacecraft power systems and thermal management.

This would require advance thermal radiatros, larger solar arrays, and possible nuclear power for outer solar system extensions.

Acquisition Time Assumptions: The 30-second baseline acquisition time assumes near-perfect platform stability and pointing knowledge. Actual spacecraft experience thermal distortions from solar heating cycles, reaction wheel vibrations at 50-200 Hz, Thruster disturbances during station-keeping, and structural flexibility in large apertures. These factors could extend acquisition times to several minutes, particularly for first-time link establishment.

Network Availability: The 99.7% connectivity achievement assumes independent failure modes and may not fully capture correlated failures from solar storms affecting multiple spacecraft, debris events from collision cascades, common-mode software failures, and manufacturing defects in component lots. Real-world availability would likely be 5-10% lower, requiring additional margin in mission planning.

Traffic Model Simplifications: Our traffic models assume predictable data generation patterns. Actual Mars missions exhibit highly bursty traffic during critical events (100× nominal), unpredictable human communication need, emergency communication requirements, and competing mission priorities. These factors could overwhelm the proposed QoS mechanisms during peak events.

Component Reliability: The simulation assumes constant failure rates without aging effects. FSO components experience laser diode degradation including 20% power loss over 5 years, ointing mechanism wear where backlash increases with cycles, detector sensitivity reduction as radiation damage accumulates, and optical surface

contamination where throughput degrades. These degradation modes could reduce system lifetime below the assumed 10-year operational period.

These limitations do not invalidate the architectural concept but suggest that performance margins should be interpreted conservatively for mission planning purposes. Future work should focus on hardware-in-the-loop testing, detailed environmental modeling, prototype relay demonstrations and international standards development.

Chapter 5
Conclusion and Future Work

This chapter synthesizes the research contributions and outlines directions for future investigation. The simulation-based feasibility study demonstrates that hierarchical FSO network architectures leveraging Lagrange point positioning could address fundamental limitations of current interplanetary communications, though significant validation work remains before operational deployment.

5.1 Research Contributions Summary

5.1.1 Primary Achievements

This research achieved its stated objectives through parametric simulation. The simulation maintained 100% modeled connectivity across a 2.28-year period using 8 Earth satellites, 4 Mars satellites, and strategically positioned relay stations at Lagrange points, demonstrating that the proposed topology could theoretically support continuous Earth-Mars communications under the assumed operating conditions. The L4/L5 relay positioning maintained simulated connectivity during solar conjunction periods when direct Earth-Mars links would be blocked, though link budgets for these longer routes require hardware validation to confirm sufficient SNR margins.

The hierarchical control system showed that navigation assistance and traffic management services could operate at 6-minute coordination cycles compatible with FSO link

timescales. Under the assumed parameter improvements—specifically 50% acquisition time reduction, 2 dB SNR enhancement, and 5% success rate increase—the simulation demonstrated potential coordination benefits, though these specific magnitudes require experimental validation. The simulation achieved aggregate data rates of 31-37 Gbps with the baseline constellation, demonstrating 5-16× improvement over current DSN capabilities (2-6 Gbps from Mars) under the modeled power (10-150W) and aperture (0.3-1.0m) constraints.

These results establish architectural feasibility under the assumed operating conditions rather than validated operational performance. The simulation framework successfully demonstrates that the proposed hierarchical architecture could maintain connectivity across representative orbital scenarios if the parametric assumptions prove accurate.

5.1.2 Novel Technical Contributions

5.1.2.1 Hierarchical Controller Architecture

This work presents the first comprehensive design integrating active controllers at Earth-Moon Lagrange points with passive relays at Sun-Earth and Sun-Mars Lagrange points for interplanetary FSO networks. The three-tier hierarchy addresses the fundamental challenge that light-speed delays (6-40 minutes Earth-Mars round-trip) prevent centralized Earth-based control. Individual satellites make local link establishment decisions based on controller guidance, while controllers at Earth-Moon L-points (L_3, L_4, L_5) provide navigation assistance and traffic coordination within seconds-scale response times. Passive relay stations at Sun-Earth and Sun-Mars L-points enable routing around solar conjunction.

The simulation demonstrates this architecture maintains network coherence across changing orbital geometries, though the specific coordination protocols require further development and the assumed controller benefits need hardware validation.

5.1.2.2 Integrated Conjunction Solution

While prior work proposed relay satellites at Lagrange points [24] [44], this research demonstrates a complete managed network architecture maintaining connectivity during conjunction periods. The simulation shows that L_4/L_5 relay positioning at both Sun-Earth and Sun-Mars systems provides continuous line-of-sight paths when direct Earth-Mars communication is blocked by the Sun. The controller coordination framework enables dynamic path selection across multiple relay options, though the assumed viable paths during peak conjunction require validation against actual link budget constraints at the extended distances.

5.1.2.3 Navigation-Assisted FSO Acquisition

The integration of controller-provided ephemeris updates and pointing recommendations represents a novel approach to FSO link acquisition across interplanetary distances. The simulation models navigation assistance using parametric assumptions: 80% acquisition success rate versus 75% baseline, 50% reduction in acquisition time from 1800s to 900s, and 2 dB SNR improvement from enhanced pointing stability. These improvements translate to the observed 55% increase in average network data rate (31.978 Gbps versus 20.215 Gbps) in the simulation.

However, these specific magnitudes represent engineering estimates extrapolated from

published research [35] [37] rather than validated performance for interplanetary FSO systems. The relationship between improved pointing accuracy and system-level benefits requires hardware demonstration to confirm.

5.1.2.4 Traffic Management Framework

The controller-based architecture implements a Quality of Service framework with five priority levels and time-slot-based scheduling. The implementation demonstrates that controllers can aggregate traffic demands, generate schedules, and communicate authorization tokens to satellites within 6-minute coordination cycles. This framework is partially integrated with link establishment logic—satellites check authorization status but may establish alternative links when scheduled relays are unavailable or when geometric factors override traffic directives.

The simulation demonstrates the architectural feasibility of controller-based traffic coordination within the hierarchical design, though full enforcement of traffic-driven link control remains future work. Performance improvements attributed to traffic coordination should be interpreted cautiously as the traffic management system is not fully integrated with the link acquisition protocols.

5.1.3 Performance Achievements Under Modeled Conditions

The simulation achieved aggregate network data rates between 31-37 Gbps with an average of 31.978 Gbps when controllers were enabled. Approximately 135 simultaneous FSO connections were maintained throughout the simulation period, with the interplanetary backbone supporting 47-78 links depending on orbital configuration.

The modeled connectivity reached 100% for both Earth and Mars networks throughout the simulation duration.

Controller coordination demonstrated significant impact on network performance. Navigation-assisted links constituted 25.4% of total connections, enabling 55% higher average throughput with controllers (31.978 Gbps versus 20.215 Gbps without controllers). Peak capacity improvement reached 55% (36.976 Gbps versus 23.859 Gbps), while maximum interplanetary links increased by 39% with controllers (78 versus 56 links).

The simulation validated scalability from initial deployment—where 8 Earth satellites and 4 Mars satellites provided 58.0% and 39.2% surface coverage respectively—to theoretical expanded constellations achieving 97.5% Earth coverage and 82.7% Mars coverage. This demonstrates the architecture's capacity for phased deployment, though the expanded constellation performance is extrapolated rather than simulated.

These achievements validates the feasibility of the core architectural concept under the assumed parameters. The modeled performance improvements depend critically on achieving the assumed navigation assistance benefits, pointing accuracy, and coordination efficiency—parameters that require hardware validation before operational deployment.

5.2 Implications for Space Exploration

5.2.1 Mission Enablement

The demonstrated network capabilities could enable mission concepts currently constrained by communication limitations, if the simulated performance translates to operational systems. High-bandwidth connectivity could support real-time telemetry during critical mission phases, interactive science operations with reduced decision latency, comprehensive data return eliminating current prioritization constraints, and high-definition video streaming for operations and public engagement. However, the light-time delay (4-24 minutes one-way) fundamentally precludes true "real-time control" as emphasized in Section 1.2.2—operations remain inherently delay-tolerant.

For human Mars missions, continuous high-bandwidth links could enable medical telemetry and telemedicine consultations, mission control support during surface operations, video communication for psychological support, and rapid technical troubleshooting. The 8-48 minute round-trip communication delay requires autonomous decision-making for time-critical situations, as discussed in Section 1.3.2.

The hierarchical architecture provides a scalable framework potentially extensible to outer solar system missions through additional relay nodes at Jupiter and Saturn systems, distributed sensor networks throughout the inner solar system, and standardized optical communication protocols enabling multi-mission resource sharing.

5.2.2 Commercial and Scientific Opportunities

The FSO network architecture could create commercial opportunities in the emerging space economy. Commercial data relay services between Earth and Mars missions could provide bandwidth leasing for scientific and commercial users, while store-and-forward services during conjunction periods would ensure continuous data flow. Traffic coordination services for constellation operators could improve efficiency, while collision avoidance coordination and inter-constellation data relay would support the growing orbital infrastructure. Emerging applications might include communication infrastructure for asteroid mining operations, high-bandwidth links for space manufacturing, and remote operation of robotic systems.

Enhanced communication capabilities could accelerate scientific discovery through comprehensive data return from high-resolution instruments without bandwidth-limited prioritization. Reduced latency for target-of-opportunity observations would enable faster response to transient phenomena, while coordinated multi-asset observations of dynamic events would improve scientific understanding. Solar system-wide sensor networks for space weather monitoring and enhanced deep space telescope operations with higher data return rates would expand our observational capabilities.

These applications assume successful validation and deployment of the proposed architecture, along with development of regulatory frameworks for commercial optical space communications.

The simulation framework provides a valuable tool for exploring architectural trade-offs and identifying critical parameters requiring hardware demonstration.

5.3 Future Research Directions

5.3.1 Critical Near-Term Validation

The highest priority work involves validating the parametric assumptions underlying the simulation. Pointing accuracy characterization through laboratory testing of FSO terminals would measure achievable pointing accuracy and its relationship to acquisition time, SNR, and success rate under various conditions. Acquisition algorithm testing using hardware-in-the-loop simulation with realistic orbital dynamics and thermal disturbances would validate navigation-assisted acquisition. Link budget verification through end-to-end testing at representative distances would confirm assumed optical efficiency (80%), beam divergence (30 μrad), and detector sensitivity. Environmental effects characterization would quantify thermal cycling, vibration, and radiation effects on FSO terminal performance over extended durations.

The simplified circular orbit propagation for access satellites should be validated against high-fidelity propagators such as GMAT or STK to quantify position errors over the 2.28-year simulation period. If errors exceed acceptable thresholds for network topology analysis, comprehensive perturbation modeling for all satellites with careful numerical conditioning should be implemented.

Completing the integration of traffic management with link establishment protocols requires implementing enforcement mechanisms where satellites prioritize traffic-scheduled links, developing conflict resolution when traffic schedules conflict with geometric constraints, measuring actual throughput improvements from traffic coordination versus autonomous operation, and characterizing the trade-offs between

coordination overhead and performance benefits.

5.3.2 Technology Demonstrations

A CubeSat demonstration mission could validate critical subsystems at lower cost and risk. The mission would test FSO terminals with navigation-assisted acquisition algorithms, controller coordination protocols between multiple spacecraft, and QoS-based traffic management under realistic orbital dynamics. On-orbit measurements of pointing jitter, thermal effects, and acquisition statistics would provide empirical data for model refinement.

An Earth-Moon L_2 relay mission would validate the architecture at intermediate distances. A controller satellite at Earth-Moon L_2 would provide regional coordination, while FSO links at 400,000 km range would demonstrate acquisition and tracking capabilities. Testing navigation assistance effectiveness in the cislunar environment would provide operational experience with hierarchical coordination protocols before interplanetary deployment.

Before full constellation deployment, a single relay at Earth-Sun L_4 or L_5 could demonstrate conjunction mitigation as a proof-of-concept with existing Mars orbiters. This mission would validate interplanetary-scale link budgets, test multi-hop routing through relays during conjunction periods, and demonstrate controller coordination across astronomical distances.

5.3.3 Advanced System Development

Future systems could incorporate adaptive optics for improved performance through wavefront sensing and correction for atmospheric links, active beam shaping for optimal power delivery, multi-aperture systems for increased capacity, and integration with navigation sensors for rapid acquisition. Machine learning techniques could enhance autonomous network management through predictive link quality estimation using orbital dynamics and historical data, adaptive routing based on learned traffic patterns, anomaly detection for early fault identification, and autonomous network reconfiguration during failures. However, ML approaches require extensive operational data for training, limiting near-term applicability.

The architecture could be extended to Jupiter and Saturn systems through additional relay stations at Jupiter-Sun and Saturn-Sun Lagrange points. Higher-power relay terminals (500W-1kW) would provide increased link margins, while larger apertures (2-3m) would overcome the inverse-square law at 5-10 AU. Nuclear power sources would enable sustained operation beyond Mars. Such extensions would require addressing the thermal management challenges, navigation accuracy degradation, and significantly extended communication delays discussed in Section 1.3.3.

5.3.4 Fundamental Research Needs

Several fundamental questions remain unresolved. Atmospheric turbulence modeling requires improved characterization of atmospheric effects on uplink and downlink segments beyond simple attenuation factors. Solar plasma effects need quantification, particularly how solar wind and coronal effects impact optical propagation during near-

Sun relay paths. Long-term component degradation must be understood, including laser diode lifetime, detector sensitivity degradation, and optical surface contamination over 10+ year missions. Coordination protocol optimization would benefit from theoretical analysis of optimal update intervals, regional coverage schemes, and fault tolerance mechanisms. Economic analysis comparing FSO constellation deployment costs to incremental RF infrastructure upgrades would inform deployment decisions.

5.4 Final Conclusions

This thesis demonstrates through parametric simulation that hierarchical FSO network architectures leveraging strategic Lagrange point positioning could theoretically address fundamental limitations of current interplanetary communications. The proposed three-tier hierarchy—comprising satellite autonomy, regional controllers at Earth-Moon L-points, and interplanetary relays at Sun-Earth and Sun-Mars L-points—maintains simulated connectivity throughout representative orbital scenarios, including solar conjunction periods. Under the assumed parameter values, the simulation demonstrates 5-16× data rate improvements over current DSN capabilities and 55% throughput gains from controller coordination. However, these improvements depend critically on achieving assumed navigation assistance benefits and pointing accuracy that require hardware validation.

Geometric analysis confirms that L_4/L_5 relay positioning maintains line-of-sight paths during solar conjunction when direct Earth-Mars links are blocked, though link budget validation for these extended routes remains necessary. The architecture supports phased deployment from initial capability through enhanced coverage to full operational

deployment, enabling incremental infrastructure development aligned with mission requirements.

5.4.1 Limitations and Required Validation

The research makes several parametric assumptions requiring experimental validation before operational deployment. Navigation assistance improvements—specifically 50% acquisition time reduction, 2 dB SNR enhancement, and 5% success rate increase—are extrapolated from published research [35] [37] rather than validated for interplanetary FSO systems. Optical efficiency values of 80% for both transmitter and receiver may be optimistic for space-qualified systems across extreme thermal cycles. Traffic coordination benefits are based on incomplete integration of traffic management with link establishment protocols. The simplified orbital mechanics for access satellites lack validation against high-fidelity propagators, while atmospheric turbulence is modeled as simple attenuation rather than dynamic beam wander and scintillation.

The simulation results demonstrate what the architecture could achieve if these assumed parameter values prove accurate, rather than validated operational performance. This parametric approach is appropriate for architectural feasibility studies but requires hardware demonstration before deployment.

5.4.2 Path Forward

The transition from simulation-based feasibility to operational systems requires a staged validation approach spanning three phases. The first phase focuses on parameter validation through laboratory and hardware-in-the-loop testing to validate assumed

FSO terminal performance, pointing accuracy, and coordination protocol effectiveness over an initial 1-3 year period. The second phase involves technology demonstrations through LEO, cislunar, and Mars precursor missions demonstrating key subsystems at progressively increasing distances and complexity over years 3-7. The third phase encompasses incremental deployment beginning with Earth-Moon controllers, followed by Sun-Earth relays, and finally Sun-Mars relay infrastructure over years 7-15.

This approach reduces technical risk while building operational experience and confidence in the architecture.

5.4.3 Broader Impact

If successfully validated and deployed, the proposed FSO network could fundamentally transform interplanetary communications. Eliminating solar conjunction blackouts would remove the current 14-day communication gaps that constrain mission operations. Providing bandwidth sufficient for comprehensive scientific data return would eliminate current prioritization constraints that force missions to discard valuable observations. Enabling high-definition video communication would support both operations and public engagement. Establishing scalable infrastructure extensible throughout the solar system would create the foundation for sustained exploration beyond Mars.

The hierarchical controller architecture addresses the fundamental challenge that light-speed delays prevent centralized Earth-based control of interplanetary networks. By positioning regional controllers at Earth-Moon Lagrange points with seconds-scale response times, the architecture enables coordinated network management impossible with purely distributed approaches or Earth-based control. However, realizing these

benefits depends on successfully validating the parametric assumptions underlying the simulation and addressing the substantial technical challenges of deploying and maintaining optical communication systems across astronomical distances in the harsh space environment.

5.4.4 Closing Remarks

This research provides a comprehensive simulation framework for evaluating hierarchical FSO interplanetary network architectures. The demonstrated feasibility under modeled conditions establishes that strategic Lagrange point positioning combined with intelligent controller coordination represents a viable approach to addressing the bandwidth and conjunction challenges limiting current space communications.

The path from simulation to operational deployment remains substantial, requiring hardware validation, technology demonstrations, and incremental infrastructure deployment over a 10-15 year timeline. Nevertheless, the architectural foundation established in this work provides a roadmap for developing the high-bandwidth, continuous-connectivity communication infrastructure necessary for sustained human presence beyond Earth and the next generation of exploration throughout the solar system.

Bibliographic references

1. Valinia, A., Allen, J. R., Francisco, D. R., Minow, J. I., Pellish, J. A. & Vera, A. H. *Safe Human Expeditions Beyond Low Earth Orbit (LEO)* Technical Memorandum NASA/TM-20220002905, NESC-RP-20-01589 (National Aeronautics and Space Administration, 2022).

2. NASA Space Science Data Coordinated Archive. *Upcoming Events* https://nssdc.gsfc.nasa.gov/planetary/upcoming.html. Curator: Dr. David R. Williams, NASA Goddard Space Flight Center. National Aeronautics and Space Administration, 2025.

3. NASA Jet Propulsion Laboratory. *Managing the Deluge of 'Big Data' From Space* Accessed: May 2025. National Aeronautics and Space Administration, 2013.

4. Hemmati, H., Biswas, A. & Djordjevic, I. B. Deep-space optical communications: future perspectives and applications. *Proceedings of the IEEE* **99,** 2020–2039. doi:10.1109/JPROC.2011.2160609 (2011).

5. *Sojourner's View of the Lander* NASA Science. https://science.nasa.gov/resource/sojourners-view-of-the-lander/ (2024).

6. Caltech Magazine. *Mars 2020: How Perseverance Rover Compares to Curiosity* https://magazine.caltech.edu/post/mars-2020-evolution-of-a-rover. 2021.

7. Wall, M. & Tillman, N. T. *Perseverance rover — Everything you need to know* https://www.space.com/perseverance-rover-mars-2020-mission. 2023.

8. Edwards Jr., C., Arnold, B., DePaula, R., Kazz, G., Lee, C. & Noreen, G. Relay communications strategies for mars exploration through 2020. *Acta Astronautica* **59,** 310–318. doi:10.1016/j.actaastro.2006.02.038 (2006).

9. Bhartia, R., Beegle, L. W., DeFlores, L., Abbey, W., Hollis, J. R., Uckert, K., *et al.* Perseverance's scanning habitable environments with raman and luminescence for organics and chemicals (SHERLOC) investigation. *Space Science Reviews* **217,** 58. doi:10.1007/s11214-021-00812-z (2021).

10. NASA. *Communications - Mars 2020 Spacecraft: Rover* Mars 2020 Mission Official Documentation. National Aeronautics and Space Administration, 2020.

11. Sandilands, S. *Talking to Martians: Communications with Mars Curiosity Rover* tech. rep. Technical analysis of Mars-Earth communications (Sandilands Consultancy, 2012).

12. Di, K., Yue, Z., Liu, Z. & Wang, S. Automated rock detection and shape analysis from Mars rover imagery and 3D point cloud data. *Journal of Earth Science* **24,** 125–135. doi:10.1007/s12583-013-0316-3 (2013).

13. Maki, J. N., Gruel, D., McKinney, C., Ravine, M. A., Morales, M., Lee, D., *et al.* The Mars 2020 engineering cameras and microphone on the Perseverance rover: a next-generation imaging system for Mars exploration. *Space Science Reviews* **216,** 137. doi:10.1007/s11214-020-00765-9 (2020).

14. NASA. *Europa Clipper Press Kit* Press Kit (National Aeronautics and Space Administration, 2024).

15. Srinivasan, D., Sheldon, C. & Bray, M. *Telecommunications systems for the NASA Europa missions* in *2017 IEEE Aerospace Conference* (2017), 394–397. doi:10.1109/AERO.2017.7943592.

16. Kessler, P., Harris, D., Prater, T. & Nickens, T. *Artemis deep space habitation: enabling a sustained human presence on the moon and beyond* in *IEEE Aerospace Conference* IEEE 978-1-6654-3760-8/22 (Huntsville, AL, 2022).

17. Gladden, R. E., Hwang, P. P., Waggoner, B. C., McLaughlin, B. A., Fieseler, P. D., Thomas, R. C., Bigwood, M. & Herrera, P. N. *Mars relay coordination lessons learned* in *2005 IEEE Aerospace Conference* IEEEAC paper #1065, Version 4 (Big Sky, MT, USA, 2005), 1–14.

18. Lent, R. Improving bundle routing in a space DTN by approximating the transmission time of the reliable LTP. *Network* **3,** 180–198. doi:10.3390/network3010009 (2023).

19. NASA Science. *Mars Relay Network* Accessed: April 2025. 2025.

20. Strauss, M. Voyager, still going after all these years. *Air & Space Magazine.* Issue: December/January 2020 (2019).

21. NASA/JPL. *Deep Space Network Services Catalog* tech. rep. DSN No. 820-100, Rev. F. JPL D-19002 (Jet Propulsion Laboratory, California Institute of Technology, 2015).

22. National Aeronautics and Space Administration. *Mars Reconnaissance Orbiter - Science Instruments* NASA Science. https://science.nasa.gov/mission/mars-reconnaissance-orbiter/science-instruments/ (2024).

23. Goh, E. *et al. Scheduling the NASA Deep Space Network with Deep Reinforcement Learning* Submitted on 9 Feb 2021. 2021. arXiv: 2102.05167 [cs.LG].

24. Howard Jr., R. L. & Seibert, M. *Lagrange-Based Options for Relay Satellites to Eliminate Earth-Mars Communications Outages During Solar Superior Conjunctions* NASA Technical Report 20205007788. NASA Technical Reports Server (NTRS) (NASA Johnson Space Center, 2020).

25. NASA Earthdata. *It's Always Sunny in Space (and That's a Problem for Satellite Teams)* NASA Earthdata Feature Article. Accessed: 2025-08-14. 2024.

26. Kontar, E. P. *et al. Plasma motions and compressive wave energetics in the solar corona and solar wind from radio wave scattering observations* 2024. arXiv: 2403.12680 [astro-ph.SR].

27. Manoharan, P. K. *Radio astronomical scintillation in the solar wind plasma: imaging interplanetary disturbances* in (2002).

28. Pennsylvania State University. *The Ionospheric Effect* GEOG 862: GPS and GNSS for Geospatial Professionals. Online course material. Department of Geography, The Pennsylvania State University, 2024.

29. NASA. *Mars Relay Network* https://science.nasa.gov/mars/mars-relay-network/. Accessed: August 14, 2025. National Aeronautics and Space Administration, 2025.

30. Cangahuala, L. A., Campagnola, S., Bradley, B. K., Boone, D. R., Buffington, B. B., Ludwinski, J. M., Nandi, S. & Scott, C. J. Europa clipper mission design, mission plan, and navigation. *Space Science Reviews* **221,** 1–53. doi:10.1007/s11214-025-01140-2 (2025).

31. NASA Science. *Cassini's Radioisotope Thermoelectric Generators (RTGs)* https://science.nasa.gov/mission/cassini/radioisotope-thermoelectric-generator/. Accessed: 2025-08-14. 2025.

32. Dunn, C., Lichten, S., Jefferson, D. & Border, J. S. *Sub-Nanosecond Clock Synchronization and Precision Deep Space Tracking* tech. rep. NASA-CR-192357. NASA Technical Reports Server ID: 19920024113 (Jet Propulsion Laboratory, California Institute of Technology, Pasadena, California, 1992).

33. Gui, M., Yang, H., Ning, X., Xiong, K., Liu, J. & Dai, M.-Z. Star angle/double-differenced pulse time of arrival integrated navigation method for Jupiter exploration. *Advances in Space Research* **71,** 2669–2678. doi:10.1016/j.asr.2022.11.006 (2023).

34. Space.com Staff. *NASA's Cassini Mission to Saturn: By the Numbers* Accessed 2025. 2017.

35. Wang, Z., Peng, C., Zhang, T., Wang, Q., Liu, S., Liu, X., Wang, Y., Huang, Y. & He, D. Space optical communication system for space optical networks and deep space exploration. *Journal of Optical Communications and Networking* **16,** 843–856. doi:10.1364/JOCN.529905 (2024).

36. Szebehely, V. *Theory of Orbits: The Restricted Problem of Three Bodies* (Academic Press, New York, 1967).

37. Hemmati, H. *Deep Space Optical Communications* (Wiley-Interscience, Hoboken, NJ, 2006).

38. Murray, C. D. & Dermott, S. F. *Solar System Dynamics* 63–129 (Cambridge University Press, Cambridge, UK, 1999).

39. Farquhar, R. W. The utilization of halo orbits in advanced lunar operations. *NASA Technical Note D-6365* (1970).

40. Whitley, R. & Martinez, R. *Options for staging orbits in cislunar space* in *IEEE Aerospace Conference* (2016), 1–9.

41. Dunham, D. W. & Roberts, C. E. Spaceguard survey: spacecraft at earth-sun libration points as observatory platforms. *Advances in Space Research* **30,** 317–324 (2002).

42. Domingo, V., Fleck, B. & Poland, A. I. The soho mission: an overview. *Solar Physics* **162,** 1–37 (1995).

43. Gardner, J. P. *et al.* The james webb space telescope. *Space Science Reviews* **123,** 485–606 (2006).

44. Jesick, M. Mars trojan orbits for continuous earth-mars communication. *The Journal of the Astronautical Sciences* **67,** 902–931. doi:10.1007/s40295-019-00195-y (2020).

45. Cornish, N. J. *The Lagrange Points* WMAP Observatory. Last updated July 2012. NASA Goddard Space Flight Center, 2012.

46. *What are Lagrange Points?* Accessed September 24, 2025. NASA Science, 2024.

47. Biswas, A., Hemmati, H. & Moision, B. Deep space optical communications: from psyche to mars. *Science* **382,** 878–882 (2023).

48. Kaushal, H. & Kaddoum, G. Optical communication in space: challenges and mitigation techniques. *IEEE Communications Surveys Tutorials* **19,** 57–96 (2017).

49. *Free-Space Optical Communication* Edmund Optics Knowledge Center. Accessed September 24, 2025. Edmund Optics.

50. Majumdar, A. K. *Free-space laser communication performance in the atmospheric channel* (Springer, 2015).

51. Hall, S. *A Survey of Free Space Optical Communications in Satellites* AE 8900 MS Special Problems Report. Space Systems Design Lab (SSDL) Technical Report (Georgia Institute of Technology, Atlanta, GA, 2020).

52. Boroson, D. M. & Robinson, B. S. The lunar laser communication demonstration: nasa's first step toward very high data rate support of science and exploration missions. *Space Science Reviews* **185,** 115–128 (2014).

53. Sun, G., Xu, G., Shao, Y., Zhang, Q. & Song, Z. Phase fluctuations-induced bit error ratio of deep-space optical communication systems during superior solar conjunction. *Optics Express* **32,** 7105–7118. doi:10.1364/OE.511003 (2024).

54. Cerf, V., Burleigh, S., Hooke, A., Torgerson, L., Durst, R., Scott, K., Fall, K. & Weiss, H. Delay-tolerant networking architecture. *RFC 4838* (2007).

55. SpaceX. *Improving Starlink's Latency* tech. rep. (SpaceX, 2024).

56. Singla, A., Calveras, A., Betorz, F. & Ruiz-De-Azua, J. A. Enhancing satellite non-terrestrial networks through advanced constellation management: optimizing in-orbit resources for nb-iot. *IEEE Open Journal of the Communications Society.* doi:10.1109/OJCOMS.2024.3384265 (2024).

57. Vallado, D. A. *Fundamentals of Astrodynamics and Applications* 4th (Microcosm Press, 2013).

58. Biswas, A. *Deep space optical communications (dsoc)* in. Government sponsorship acknowledged (Pasadena, CA, 2018).

59. Scott, K. L. & Burleigh, S. *Bundle Protocol Specification* RFC 5050. Experimental. 2007. doi:10.17487/RFC5050.

60. Boroson, D. M. & Robinson, B. S. *Mars laser communications demonstration design* in *IEEE Aerospace Conference* (2014), 1–11.

61. Cornwell, D. M. *Nasa's optical communications program* in *Free-Space Laser Communication and Atmospheric Propagation XXVIII* **9739** (2016), 97390E.

62. Raza, W., Abele, E., O'Hara, J., Sadr, B., LoPresti, P., Imran, A., Choi, W., Song, I., Altunc, S., Kegege, O. & Ekin, S. Towards a hybrid rf/optical lunar communication system (lunarcomm). *arXiv preprint arXiv:2203.15899.* Submitted to IEEE (2022).

63. Castellini, F., Simonetto, A., Martini, R. & Lavagna, M. A mars communication constellation for human exploration and network science. *Advances in Space Research* **45,** 183–199. doi:10.1016/j.asr.2009.10.019 (2010).

64. Xu, G. & Song, Z. Amplitude fluctuations for optical waves propagation through non-kolmogorov coronal solar wind turbulence channels. *Optics Express* **26,** 8566–8580. doi:10.1364/OE.26.008566 (2018).

Appendix A
Mathematical Derivations

A.1 Lagrange Point Calculations

A.1.1 Lagrange Point Calculations

For collinear Lagrange points (L_1 and L_2), the distances are calculated using the mass ratio μ and the cubic approximation:

$$\mu = \frac{m_2}{m_1 + m_2} \tag{A.1}$$

$$r_{L1} \approx r\left(1 - \left(\frac{\mu}{3}\right)^{1/3}\right) \tag{A.2}$$

$$r_{L2} \approx r\left(1 + \left(\frac{\mu}{3}\right)^{1/3}\right) \tag{A.3}$$

For triangular points (L_4 and L_5), they form equilateral triangles with the two primary bodies:

$$r_{L4} = r_{L5} = r \tag{A.4}$$

where r is the distance between the two primary bodies.

A.1.2 Earth-Sun System

System Parameters:

$$\mu_{Earth-Sun} = \frac{1}{332,946} \tag{A.5}$$

$$r = 1 \text{ AU} = 149,597,870.7 \text{ km} \tag{A.6}$$

$$\left(\frac{\mu}{3}\right)^{1/3} = \left(\frac{1}{998,838}\right)^{1/3} \approx 0.01000125 \tag{A.7}$$

Distance Calculations:

$$\text{Earth to } L_1: \quad d_{E-L1} = r \cdot \left(\frac{\mu}{3}\right)^{1/3} \tag{A.8}$$

$$= 149,597,870.7 \times 0.01000125 \tag{A.9}$$

$$\approx \boxed{1,496,000 \text{ km}} \tag{A.10}$$

$$\text{Earth to } L_2: \quad d_{E-L2} = r \cdot \left(\frac{\mu}{3}\right)^{1/3} \tag{A.11}$$

$$= 149,597,870.7 \times 0.01000125 \tag{A.12}$$

$$\approx \boxed{1,496,000 \text{ km}} \tag{A.13}$$

$$\text{Earth to } L_4: \quad d_{E-L4} = r = \boxed{149,597,871 \text{ km}} \tag{A.14}$$

$$\text{Earth to } L_5: \quad d_{E-L5} = r = \boxed{149,597,871 \text{ km}} \tag{A.15}$$

A.1.3 Earth-Moon System

System Parameters:

$$\mu_{Earth-Moon} = \frac{1}{81.30056} \tag{A.16}$$

$$r = 384,400 \text{ km (mean Earth-Moon distance)} \tag{A.17}$$

$$\left(\frac{\mu}{3}\right)^{1/3} = \left(\frac{1}{243.90168}\right)^{1/3} \approx 0.15870 \tag{A.18}$$

Distance Calculations:

$$\text{Earth to } L_1: \quad d_{E-L1} = r \cdot \left(1 - \left(\frac{\mu}{3}\right)^{1/3}\right) \tag{A.19}$$

$$= 384,400 \times (1 - 0.15870) \tag{A.20}$$

$$\approx \boxed{323,500 \text{ km}} \tag{A.21}$$

$$\text{Earth to L}_2: \quad d_{E-L2} = r \cdot \left(1 + \left(\frac{\mu}{3}\right)^{1/3}\right) \tag{A.22}$$

$$= 384,400 \times (1 + 0.15870) \tag{A.23}$$

$$\approx \boxed{445,300 \text{ km}} \tag{A.24}$$

$$\text{Earth to L}_4: \quad d_{E-L4} = r = \boxed{384,400 \text{ km}} \tag{A.25}$$

$$\text{Earth to L}_5: \quad d_{E-L5} = r = \boxed{384,400 \text{ km}} \tag{A.26}$$

A.1.4 Mars-Sun System

System Parameters:

$$\mu_{Mars-Sun} = \frac{1}{3,098,708} \tag{A.27}$$

$$r = 1.524 \text{ AU} = 227,943,824 \text{ km} \tag{A.28}$$

$$\left(\frac{\mu}{3}\right)^{1/3} = \left(\frac{1}{9,296,124}\right)^{1/3} \approx 0.004745 \tag{A.29}$$

Distance Calculations:

$$\text{Mars to } L_1: \quad d_{M-L1} = r \cdot \left(\frac{\mu}{3}\right)^{1/3} \tag{A.30}$$

$$= 227,943,824 \times 0.004745 \tag{A.31}$$

$$\approx \boxed{1,082,000 \text{ km}} \tag{A.32}$$

$$\text{Mars to } L_2: \quad d_{M-L2} = r \cdot \left(\frac{\mu}{3}\right)^{1/3} \tag{A.33}$$

$$= 227,943,824 \times 0.004745 \tag{A.34}$$

$$\approx \boxed{1,082,000 \text{ km}} \tag{A.35}$$

$$\text{Mars to } L_4: \quad d_{M-L4} = r = \boxed{227,943,824 \text{ km}} \tag{A.36}$$

$$\text{Mars to } L_5: \quad d_{M-L5} = r = \boxed{227,943,824 \text{ km}} \tag{A.37}$$

A.2 FSO Link Budget Equations

A.2.1 Majumdar Link Budget Equation

The complete FSO link budget follows Majumdar's fundamental equation [**majumdar2005**]:

$$P_{REC} = P_T \cdot G_T \cdot \tau_T \cdot \tau_{ATM} \cdot S \cdot G_R \cdot \tau_R \tag{A.38}$$

where P_T is transmitted power, G_T is transmitter gain, τ_T is transmitter efficiency, τ_{ATM} is atmospheric transmission, S is free-space loss factor, G_R is receiver gain, and τ_R is receiver efficiency.

A.2.2 Transmitter Optical Gain

The transmitter gain is given by Majumdar's formula:

$$G_T = \frac{16}{\theta_T^2} \tag{A.39}$$

where θ_T is the full transmitting divergence angle in radians. In dB:

$$G_T[\text{dB}] = 10 \log_{10}\left(\frac{16}{\theta_T^2}\right) = 12.04 - 20 \log_{10}(\theta_T) \tag{A.40}$$

For a typical space-qualified laser with $\theta_T = 30$ μrad:

$$G_T = \frac{16}{(30 \times 10^{-6})^2} = 1.78 \times 10^{10} \approx 102.5 \text{ dB} \tag{A.41}$$

A.2.3 Receiver Optical Gain

The receiver gain for a circular aperture is:

$$G_R = \left(\frac{\pi D}{\lambda}\right)^2 \tag{A.42}$$

where D is the receiver diameter and λ is the wavelength. In dB:

$$G_R[\text{dB}] = 20\log_{10}\left(\frac{\pi D}{\lambda}\right) \tag{A.43}$$

For $D = 1$ m and $\lambda = 1550$ nm:

$$G_R = \left(\frac{\pi \times 1}{1550 \times 10^{-9}}\right)^2 = 4.11 \times 10^{12} \approx 126.1 \text{ dB} \tag{A.44}$$

A.2.4 Free-Space Loss Factor

The free-space loss factor (not in dB) is:

$$S = \left(\frac{\lambda}{4\pi L}\right)^2 \tag{A.45}$$

where L is the range. The corresponding path loss in dB is:

$$L_{fs}[\text{dB}] = -10\log_{10}(S) = 20\log_{10}\left(\frac{4\pi L}{\lambda}\right) \tag{A.46}$$

For $L = 1$ AU (1.496×10^{11} m) and $\lambda = 1550$ nm:

$$L_{fs} = 20 \log_{10} \left(\frac{4\pi \times 1.496 \times 10^{11}}{1550 \times 10^{-9}} \right) \approx 260.4 \text{ dB} \tag{A.47}$$

A.2.5 Atmospheric Transmission

For space-based communications, atmospheric effects are minimal:

$$\tau_{ATM} = \begin{cases} 1.0 & \text{space-to-space links} \\ 0.95 & \text{GEO satellite links} \\ 10^{-\alpha L/10} & \text{atmospheric paths} \end{cases} \tag{A.48}$$

where α is the attenuation coefficient (dB/km) and L is the atmospheric path length (km).

A.2.6 Optical Efficiencies

Transmitter and receiver optical efficiencies account for:

$$\tau_T = \eta_{laser} \cdot \eta_{optics} \cdot \eta_{pointing} \approx 0.8 \tag{A.49}$$

$$\tau_R = \eta_{detector} \cdot \eta_{optics} \cdot \eta_{coupling} \approx 0.8 \tag{A.50}$$

A.2.7 Data Rate Capability

Majumdar's data rate equation:

$$R = \frac{P_t \tau_{opt} \tau_{ATM} A}{\pi(\theta_t/2)^2 L^2 E_p N_b} \tag{A.51}$$

where A is receiver aperture area, $E_p = hc/\lambda$ is photon energy, N_b is photons per bit, and $\tau_{opt} = \tau_T \tau_R$.

For space communications with $N_b = 100$ photons/bit:

$$E_p = \frac{hc}{\lambda} = \frac{6.626 \times 10^{-34} \times 2.998 \times 10^8}{1550 \times 10^{-9}} = 1.28 \times 10^{-19} \text{ J} \tag{A.52}$$

A.2.8 Link Margin

Majumdar's link margin formula:

$$M = \frac{P_T}{N_b R h \nu} \cdot \frac{D^2}{\theta_T^2 L^2} \cdot \tau_T \cdot 10^{-\alpha L/10} \cdot \tau_R \tag{A.53}$$

In dB form:

$$M[\text{dB}] = P_T[\text{dBm}] + G_T[\text{dB}] + \tau_T[\text{dB}] + \tau_{ATM}[\text{dB}] - L_{fs}[\text{dB}] + G_R[\text{dB}] + \tau_R[\text{dB}] - P_{req}[\text{dBm}] \tag{A.54}$$

A.2.9 Complete Link Budget

The total received power in dBm:

$$P_r[\text{dBm}] = P_t[\text{dBm}] + G_t[\text{dB}] + \tau_T[\text{dB}] + \tau_{ATM}[\text{dB}] - L_{fs}[\text{dB}] + G_r[\text{dB}] + \tau_R[\text{dB}] \quad \text{(A.55)}$$

Note: While the complete Majumdar equations are implemented for link budget calculations and reporting, operational link quality decisions use simplified SNR-based thresholds for computational efficiency.

Appendix B

FSO Terminal and Component Specifications

B.1 FSO Terminal Configuration by Satellite Type

Table B.1: FSO Terminal Specifications

Parameter	**Access Satellite**	**Controller**	**Relay**
Aperture Size	0.3 m	0.5 m	1.0 m
Laser Power	10 W	50 W	150 W
Wavelength	1550 nm	1550 nm	1550 nm
Beam Divergence	30.0 μrad	30.0 μrad	30.0 μrad
Pointing Accuracy	10.0 μrad	10.0 μrad	10.0 μrad
Max Simultaneous Links	2	4	10
Baseline Acquisition Time	30 min	30 min	30 min
Baseline Data Rate	1 Gbps	1 Gbps	1 Gbps

B.2 Link Quality and Performance Parameters

Table B.2: FSO Link Quality Classifications

Quality Level	**Quality Factor**	**SNR (dB)**	**Data Rate**
Excellent	0.95	>10	1.0 Gbps
Good	0.85	5-10	0.8 Gbps
Degraded	0.70	0-5	0.5 Gbps
Poor	0.50	-5-0	0.2 Gbps

Table B.3: Navigation Assistance Performance Improvements

Metric	**Without Navigation**	**With Navigation**
Acquisition Time	30 min	15 min (50% reduction)
Acquisition Success Rate	75%	80% (+5%)
Pointing Error	10.0 μrad	5.0 μrad (50% reduction)
SNR Enhancement	Baseline	+2 dB
Processing Delay	0.1 ms	0.08 ms (20% reduction)

B.3 Traffic Management Parameters

Table B.4: QoS Priority Levels and Scheduling

Priority Level	**Scheduling Target**	**Typical Use Case**
EMERGENCY	Immediate	Safety-critical commands
CRITICAL	Within 3 minutes	System control messages
HIGH	Within 15 minutes	Science data bursts
NORMAL	Best effort	Regular telemetry
LOW	Background	Bulk data transfers

Appendix C

Simulation Parameters and Configuration

C.1 Physical Constants and Orbital Parameters

Table C.1: Celestial Body Parameters and Mass Ratios

Parameter	**Value**	**Units**
Celestial Body Radii		
Earth Radius	6,371.0	km
Mars Radius	3,389.5	km
Moon Radius	1,737.4	km
Sun Radius	695,700.0	km
Orbital Distances		
Astronomical Unit (AU)	149,597,870.7	km
Earth-Mars Closest	0.372	AU
Earth-Mars Farthest	2.675	AU
Earth-Moon Distance	384,400	km (mean)
Mass Ratios (μ)		
Earth-Moon System	1/81.30056	-
Earth-Sun System	1/332946.0	-
Mars-Sun System	1/3098708.0	-

C.2 FSO System Configuration

Table C.2: FSO Communication System Parameters

Parameter	**Value**	**Units**
Optical System		
Wavelength	1550	nm
Beam Divergence	20.0	μrad
Pointing Accuracy	10.0	μrad
Baseline Data Rate	1.0	Gbps
Environmental Factors		
Solar Exclusion Radius	5.0 $\times$ Solar Radius	km
Communication Ranges		
Maximum FSO Range	1.0	AU
Controller Coverage	0.5	AU
Deep Space Relay Range	1.0	AU

C.3 Network Architecture Configuration

Table C.3: Network Constellation and Timing Parameters

Parameter	**Value**	**Units**
Constellation Size		
Earth Satellites (GEO)	8	satellites
Mars Satellites (Areostationary)	4	satellites
Earth-Moon Controllers	3	L3, L4, L5
Earth-Sun Relays	4	L1, L2, L4, L5
Mars-Sun Relays	4	L1, L2, L4, L5
Simulation Timing		
Simulation Duration	20,000	hours
Time Step	0.25	hours (15 min)
Navigation Update Interval	0.1	hours (6 min)
Traffic Update Interval	0.05	hours (3 min)
Transmission Slot Duration	0.02	hours (1.2 min)
Prediction Horizon	2.0	hours
Coordination Parameters		
Handoff Threshold	0.8	quality factor
Link Drop Threshold	0.1	quality factor
Cache Expiry Time	1.0	hours

C.4 Validation Test Configuration

Table C.4: Validation Test Parameters

Test Scenario	**Parameter**	**Value**
Solar Conjunction Test		
Earth Position	[1.0, 0, 0]	AU
Mars Position	[-1.52, 0, 0]	AU
Conjunction Angle	180	degrees
Link Failure Recovery		
Maximum Failures	5	links
Recovery Probability	30%	per 6 min
Recovery Target	95%	connectivity
Maximum Attempts	10	-
Traffic Overload Test		
Overload Factor	2.5×	baseline
Emergency Data Size	50	MB
Science Data Burst	0.5-5.0	GB
Regular Telemetry	100	MB/2hr
Ephemeris Configuration		
Ephemeris Version	DE440	JPL
Base Date	2025-05-03 12:00:00	UTC
Position Accuracy	<1	km

Appendix D
Implementation Code

This appendix references the implementation of the FSO interplanetary network simulation framework. The complete implementation (4,944 lines) is contained in a single file available at:

https://github.com/nickyduesxd/Masters_Thesis

The implementation sections referenced in Chapter 3 can be found at the following line numbers in `model.py`:

D.1 Import Statements and Constants

Lines 1–64: Import statements and global constants including:

D.2 Core Satellite Class

Lines 65–691: `Satellite` class

Lines 1202–1299 `EnhancedSatellite` class

D.3 Celestial Mechanics and Ephemeris Classes

Lines 836–905: `LineOfSightChecker` class

Lines 909–945: `RealEphemerisData` class

Lines 948–1199: `PreciseLagrangePoints` class

D.4 Traffic Management System

Lines 821–870: Core traffic classes:

Lines 1275–1299 : `TrafficQueue` class

Lines 1301–1328 : `TransmissionSchedule` class

Lines 693–730 : `InterControllerCoordinator` class

Lines 815–833 : `SchedulingIntention` class

D.5 Metrics Collection System

Lines 1330–2013: `ThesisMetricsCollector` class

D.6 Coordination and Communication Classes

Lines 2375–2387: `TrafficCoordinationUpdate` class

Lines 2390–2396: `NavigationUpdate` class

D.7 Realistic Orbital Mechanics

Lines 2399–2530: `RealisticOrbitalMechanics` class

D.8 Navigation Coordination System

Lines 2555–2804: `NavigationCoordinator` class

D.9 FSO Terminal

Lines 2807–3145: `FSO_Terminal` class

D.10 Network Architecture

Lines 3148–4242: `FSO_NetworkArchitecture` class

D.11 Validation Test Functions

Lines 4245–4304: `test_simple_connectivity` function

Lines 4318–4352: `test_controller_coordination` function

Lines 4355–4538: `test_solar_conjunction` function

Lines 4541–4607: `test_dynamic_link_failure_recovery` function

Lines 4610–4669: `test_traffic_overload_scenario` function

Lines 4672–4724: `test_orbital_configuration_impact` function

D.12 Main Simulation Function

Lines 4856–4941: `run_fso_network_simulation` function